M&D Modelle & Daten

Technical Report

No. 2

Support for Climate- and Earth System Research at the Max Planck Institute for Meteorology, Hamburg

Climatology and Internal Variability in a 1000-Year Control Simulation with the Coupled Climate Model ECHO-G

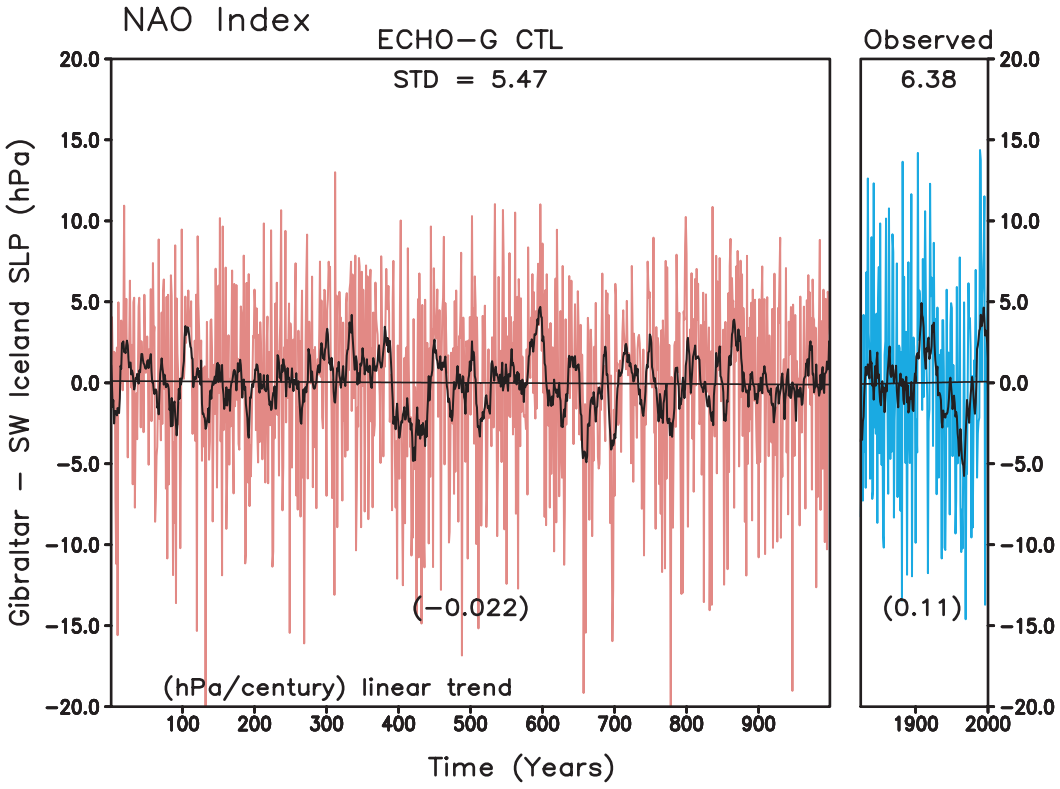

by

Seung-Ki Min • Stephanie Legutke

Andreas Hense • Won-Tae Kwon

Hamburg, March 2004

Support for Climate- and Earth System Research at the Max Planck Institute for Meteorology, Hamburg

Postal:

Modelle und Daten

Max-Planck Institut für Meteorologie

Bundesstrasse 53
D-20146 Hamburg
Germany

Office:

Tel.: +49 - (0)40 411 73 - 397

Fax: +49 - (0)40 411 73 - 476

e-mails:

Office: mad_office@dkrz.de

Data Section: data@dkrz.de

Model Section: model@dkrz.de

Internet:

Home Page: http://www.mpimet.mpg.de/Depts/MaD/

Cover figure: Time series of DJFM mean NAO index anomalies (thin lines) from ECHO-G CTL and observations (1825/26-2001/02). Solid lines are linear trends. Their values are given in parentheses (hPa/century). Thick lines are 11-year moving averages.

Technical Report

No. 2

Gruppe Modelle & Daten

Support for Climate- and Earth System Research at the Max Planck Institute for Meteorology, Hamburg

Climatology and Internal Variability in a 1000-Year Control Simulation with the Coupled Climate Model ECHO-G

Seung-Ki Min[*1], Stephanie Legutke[2], Andreas Hense[1], Won-Tae Kwon[3]*

[1]*Meteorologisches Institut*
Universität Bonn, Germany

[2]*Modelle & Daten*
Max-Planck-Institut für Meteorologie
Hamburg, Germany

[3]*Meteorological Research Institute*
Korea Meteorological Administration
Seoul, Korea

This series also appears in printed form (ISSN 1619-2249)

ISSN 1619-2257

Hamburg, March 2004

Climatology and Internal Variability in a 1000-Year Control Simulation with the Coupled Climate Model ECHO-G

Seung-Ki Min*[1], Stephanie Legutke[2], Andreas Hense[1], Won-Tae Kwon[3]

[1]Meteorologisches Institut, Universität Bonn, Germany
[2]Modelle & Daten, Max-Planck-Institut für Meteorologie, Hamburg, Germany
[3]Meteorological Research Institute, Korea Meteorological Administration, Seoul, Korea

March 1, 2004

*Corresponding author: Seung-Ki Min, Meteorologisches Institut, Universität Bonn, Auf dem Hügel 20, 53121 Bonn, Germany, E-mail: skmin@uni-bonn.de

Abstract

The climatology and internal variability in a 1000-year control simulation of the coupled atmosphere-ocean global climate model ECHO-G are analyzed and compared with observations and other coupled climate model simulations. ECHO-G requires annual mean flux corrections for heat and freshwater in order to simulate no climate drift for 1000 years, but no flux corrections for momentum. The ECHO-G control run captures well most aspects of the observed seasonal and annual climatology and of the interannual to decadal variability. Model biases are very close to those in ECHAM4 stand-alone integrations with prescribed observed sea surface temperature. A trend comparison between observed and modeled near surface temperatures shows that the observed global warming at near surface level is beyond the range of internal variability produced by ECHO-G.

The simulated global mean near surface temperatures, however, show a two-year spectral peak which is linked with a strong biennial bias of energy in the ENSO signal. Consequently, the interannual variability (3-9 years) is underestimated. The overall ENSO structure such as the tropical SST climate and its seasonal cycle, a single ITCZ in the eastern tropical Pacific, and the ENSO phase-locking to the annual cycle are simulated reasonably well by ECHO-G. However, the amplitude of SST variability is overestimated in the eastern equatorial Pacific and the observed westward propagation of zonal wind stress over the equatorial Pacific is not captured by the model. ENSO-related teleconnection patterns of near surface temperature, precipitation, and mean sea level pressure are reproduced realistically. The station-based NAO index in the model exhibits a 'white' noise spectrum similar to the observed and the NAO-related patterns of near surface temperature, precipitation, and mean sea level pressure are also simulated successfully. However, the model overestimates the additional warming over the North Pacific in the high index phase of the NAO, a feature it shares with other coupled models and which might be associated with an enhanced Atlantic-Pacific teleconnection which is hardly seen in the observations. A detection analysis of the NAO index shows that the observed recent 40-60 year trend cannot be explained by the model internal variability while the recent 20-30 year trend occurs with a more than 1% chance in ECHO-G CTL.

1. Introduction

The knowledge of internal climate variability is not only necessary for climate change detection and attribution studies, but also fundamental for climate change projection and model evaluation (e.g. Collins et al. 2001). The instrumental observational records are known to be insufficient for a proper estimation of internal climate variability due to their short temporal and spatial coverage. Also they are contaminated by unknown external forcing, e.g. volcanic eruptions, changes in solar output as well as the anthropogenic emission of greenhouse gases (Stouffer et al. 2000). Although proxy climate data such as tree-rings, historical documents, and sediments provide important information for the past climate on large time scales, they are too sparse spatially to give accurate global signals (e.g. Barnett et al. 1999). As a surrogate, atmosphere-ocean coupled general circulation models (AOGCMs) have been used widely for climate studies.

Studies of climate variability on annual to decadal time scales require simulation lengths of O(1000a). There have been several more than 1000-year control integrations (i.e. with fixed external forcing; see Table 1): GFDL_R15_a, ECHAM1/LSG, ECHAM3/LSG, HadCM2, HadCM3, and CSIRO_Mk2 which were performed at the Geophysical Fluid Dynamics Laboratory (GFDL), the German Climate Computer Centre (Deutsches Klimarechenzentrum, DKRZ), the United Kingdom Met Office (UKMO), and the Commonwealth Scientific and Industrial Research Organization (CSIRO), respectively. All model runs except for HadCM3 use flux-corrections. The climatology and variability in control runs of each model have been analyzed and compared with observations (see the references in Table 1) and intercomparisons between model runs have been carried out in terms of internal variability of near surface temperature (Stouffer et al. 2000; Braganza et al. 2002) and various atmospheric and oceanic variables (von Storch et al. 2000, 2001).

Recently a 1000-year control integration with ECHO-G (CTL), an AOGCM developed by the Model and Data group (M&D) at the Max Planck Institute for Meteorology (MPIfM), has been carried out. The atmospheric component of ECHO-G is ECHAM4 (Roeckner et al. 1996a) and the oceanic component is HOPE-G (Legutke and Maier-Reimer 1999). The objective of this paper is to describe the climatology and internal variability of an ECHO-G control run and to validate them by comparison with observations. In addition to the climatology of surface variables, the simulation skill for two dominant phenomena of natural climate variability, the El Niño Southern Oscillations (ENSO) and North Atlantic Oscillations (NAO), are evaluated. Additionally ECHO-G performances are compared with those of other AOGCMs analyzed in the Coupled Model Intercomparison Project 1 (CMIP1) (Lambert and Boer 2001; AchutaRao and Sperber 2002; Stephenson and

Pavan 2003) and the Climate Variability and Predictability Project (CLIVAR) (Latif et al. 2001; Davey et al. 2002). This paper will be a background for future studies of climate change detection and projections using ECHO-G ensemble simulations with Intergovernmental Panel on Climate Change (IPCC) scenarios.

ECHO-G, the integration method of the control simulation, and the observational datasets used for model validation are described in the next section. The climatology and variability of surface variables in ECHO-G CTL are compared with observations in Section 3. The model ENSO and NAO simulations are evaluated in Section 4 and 5, respectively. A summary of analysis results is given in the last section with some discussions.

2. Model and observations

2.1 Model description

ECHO-G consists of two component models, the atmospheric component ECHAM4 and the oceanic component HOPE-G. ECHAM4 is the fourth generation version of the Hamburg atmospheric general circulation model (AGCM), which was modified from the European Centre for Medium-Range Weather Forecasts (ECMWF) AGCM for the use in long-term climate simulations at the Max Planck Institute for Meteorology. A general model description and validation of the present-day climate simulations with ECHAM4 are given by Roeckner et al. (1996a). The standard ECHAM4 has been modified for ECHO-G such that the heat, freshwater, and momentum fluxes are calculated separately for the ice-covered and the ice-free part of each ocean grid cell following Grötzner et al. (1996). To close the freshwater and heat budgets, a scheme for continental and river runoff and ice discharge from continental ice sheets has been implemented (Legutke and Voss 1999a). The formulation of the ice discharge, which includes the release of latent heat of fusion associated with a mass discharge from the continental ice sheets of Greenland and Antarctica to close the heat budget in the coupled system, was shown to greatly improve the bottom water formation near the Antarctic coast (Legutke 2000).

It has been shown that ECHAM4 performs well on a T30 grid relative to the standard version on a T42 grid (triangular truncation 30/42) (Stendel and Roeckner 1998). In addition, HOPE-G showed overall similar performance when forced by T30 ECHAM4 model data or T42 data (Legutke et al. 1996). Therefore, the T30 grid version (about 3.75°) of ECHAM4 is used for the 1000-year control integration in order to gain considerable computational time. The vertical resolution of ECHAM4 is defined by 19 hybrid sigma-pressure levels with the highest level at 10 hPa.

The ocean model HOPE-G is the global version of the Hamburg Ocean Primitive

Equation Model (HOPE) and includes a dynamic-thermodynamic sea-ice model with a viscous-plastic rheology (Hibler 1979) and a snow cover. A gaussian T42 grid (about 2.8°) is used with a gradual meridional refinement reaching 0.5° in the tropical oceans between 10°S and 10°N. The vertical resolution is given by 20 horizontal levels with eight levels within the top 200 meters from the ocean surface. HOPE-G has been little changed from Wolff et al. (1997) except for the thermodynamic ice growth, which is computed from the fluxes obtained from the atmospheric model rather than from heat-balance equations based on bulk formulas. The climatology of HOPE-G forced by atmospheric fluxes obtained by an experiment with ECHAM4 using Atmospheric Model Intercomparison Project (AMIP) sea surface temperature (SST) is described in detail by Legutke and Maier-Reimer (1999).

ECHAM4 and HOPE-G are coupled by the OASIS software (Valcke et al. 2000). They exchange 10 daily mean atmospheric fluxes (zonal and meridional momentum flux over water and over ice, solid freshwater flux over ice, liquid freshwater flux, downwelling solar heat flux, net heat flux over water, conductive and residual heat flux over ice) and four surface conditions (SST, sea ice concentration and thickness, snow depth) once a day. The model time steps are 30 minutes for ECHAM4 and 12 hours for HOPE-G. A more detailed description of the coupling techniques of ECHO-G can be found in Legutke and Voss (1999a). ECHO-G is a descendant of the coupled GCM ECHO-1 (Latif et al. 1994; Latif and Barnett 1994, 1996; Schneider et al. 1996; Grötzner et al. 1998) and ECHO-2 (Frey et al. 1997; Pierce et al. 2000; Venzke et al. 2000). The ancestor models (ECHO-1 and ECHO-2) did not include a sea-ice component but relaxed SSTs to observed climatological values poleward of 60°.

2.2 Control simulation

After a stand-alone integration of 18 years of the atmosphere and 2034 years of the ocean, an initial coupled integration of 155 years was done. In this initial spinup, SST and sea surface salinity (SSS) were relaxed to seasonal climatological values. However, no salinity relaxation was applied in the AMIP climatological sea-ice regions to avoid distortion of the upper-ocean salinity changes related to ice production (Legutke and Cubasch 2000). Annual mean heat and freshwater fluxes, as diagnosed from the relaxation terms during the last 100 years of the coupled spinup phase, are used as flux corrections for the control simulation. Both flux fields are normalized to vanish globally. No momentum flux corrections are applied. This flux correction method has the merit of leaving the seasonal cycle and the wind stress determined by model, as well as freshwater fluxes in sea ice regions related to the ice melting and freezing processes.

The ECHO-G CTL data has been used for some recent climate variability studies.

Baquero-Bernal et al. (2002) investigated the dependence of the Indian Dipole mode on the ENSO, comparing the first 100 years from the control run with a 100-year simulation in which the ENSO variability was suppressed by relaxation to climatological mean model SST. Zorita et al. (2003) assessed an uncertainty in a paleoclimate reconstruction method. Marsland et al. (2003) examined the variability of the Antarctic Circumpolar Wave and Rodgers et al. (2004) analyzed decadal modulations of ENSO.

2.3 Observation-based data

The observational data used in this study are listed in Table 2 for each variable with source, resolution, analysis period, and key references. Near surface temperature (T2m), precipitation (PCP), and mean sea level pressure (MSLP) are regarded as 'basic' surface variables. T2m is obtained from the Climate Research Unit (CRU). Two datasets are used as PCP observations: the Merged Analysis Precipitation (CMAP) of the CPC (Climate Prediction Center) and the CRU-PCP data. The National Centers for Environmental Prediction (NCEP) and the National Center for Atmospheric Research (NCAR) provided reanalysis of MSLP. In addition, zonal wind stress data obtained from the Southampton Oceanography Centre (SOC) as well as the NINO3 index defined as the spatial mean SST anomaly in the NINO3 region evaluated from the Global sea Ice and Sea Surface Temperature (GISST) dataset for the period of 1903-1994 are used for evaluation of the model ENSO simulation. For NAO analysis we use a non-normalized index defined as the difference of DJFM mean MSLPs between Gibraltar and Southwest Iceland (Jones et al. 1997). T2m, PCP, and MSLP from the model simulations and observations are interpolated onto a common 5°×5° grid before analysis. The global mean is defined as the area-weighted average between 85°S and 85°N of the interpolated data.

The observations of HadCRUT and CRU-PCP have space and time varying missing data points, while the model has no missing data. Also, the observations represent a shorter time period than the 1000 years of model control data. Therefore, the model data on grid points where observational data are missing, are treated as missing and are referred to as 'masked' model data, and the 1000-years of ECHO-G CTL are divided into subperiods with the same length as the observational period.

3. Climatology and variability of surface variables

The overall performance of ECHO-G is described now for the basic surface variables, that is T2m (including SST), PCP, and MSLP. Not only the long-term climatology including global and zonal mean patterns, but also the spatial patterns of interannual variability and the

power spectra are compared with the observations.

3.1 Near surface temperature

The global mean T2m retain a seasonal cycle due to the hemispheric differences of land-sea distribution. The annual (ANN), June to August (JJA), and December to February (DJF) mean time series of global mean T2m are shown in Figure 1. Corresponding observed values (estimated from the 1961-1990 climate of HadCRUT, Jones et al. 1999) are 14.1, 15.9, and 12.4°C, respectively. Thus the ECHO-G model climate is somehow warmer (0.3-0.5˚C) than the observed. No significant drift in surface temperature occurs in the ECHO-G climate (-0.003°C/century). In contrast, observed temperatures show a positive trend of 0.47°C/century (see Fig. 2). The standard deviation (STD) of linearly detrended global mean T2m of ECHO-G CTL is 0.11°C, which is smaller than the STD of the detrended observed T2m which is 0.14°C.

The power spectra of global mean T2m is compared with the observed following the method used by Collins et al. (2001). The monthly global temperature anomaly time series from the 1000-year control run is divided into ten 100-year periods and the space-time varying missing-data information from the observational data (HadCRUT, 1901-2000) are used to mask the model data. The power spectra of area-weighted global mean temperatures are calculated, after the linear trends have been removed, for each 100-year time series of the model data subsections and for the observations. Figure 3 shows the power spectra of the global mean temperature. While the power spectra of the observations have no significant peak against an AR(1) process (Hasselmann 1976), a statistically significant 2-year peak appears in the model data. According to Gillett et al. (2000) the model data and the observations are significantly different at the 93% level (ln 2 / 10 independent subsections) in the periods of around 2 and 3-9 years. The model has more energy in the 2-year period and less power in the period of 3-9 years than the observations. These spectral characteristics of the modeled T2m are related to a strong 2-year periodicity in the ENSO variability (see section 4.1).

Considering that the decadal variability of global mean T2m in ECHO-G CTL is compared well to observations (Fig. 3), we investigated the probability of the occurrence of trends greater than the observed trends following Collins et al. (2001) (Table 3). Numbers of trend occurrences in ECHO-G CTL are obtained from moving windows for specified periods. The maximum observed trend of 3.2°C/century appears in the recent 10-year period (1992-2001). There is a 2.3% chance of finding a larger trend in ECHO-G CTL. For periods of 20 years and longer, there is no occurrence in the model of trends larger than the maximum observed value, which is consistent with the HadCM3 results of Collins et al.

(2001). This result holds for the ‘masked’ and ‘unmasked’ model data (see the values in parentheses in Table 3).

Figure 4 and 5 show the geographical patterns of DJF and JJA T2m, respectively, of the model and observations, as well as their zonal mean difference. The simulated T2m, which most AOGCMs are known to simulate well (e.g. Lambert and Boer 2001), are very similar to the observed, both for the geographical and zonal mean patterns. The zonal mean temperature distributions display cold biases in the Northern Hemisphere (NH) high latitudes, while warm biases appear in the Southern Ocean (SO). Note that the T2m are strongly dependent on the presence of an ice cover in ocean cells. The Arctic domain and the Himalayan mountain ranges are dominated by cold biases. The Arctic cold bias in JJA is a feature opposite to the warm bias in the ECHAM4 simulations with prescribed observed SSTs (Roeckner et al. 1996a). Warm biases are significant over mid-latitude continental areas of both hemispheres during DJF, while cold biases appear in NH mid-latitude continents in JJA. The JJA cold bias on the Asian continent indicates a decreased land-sea contrast and may account partly for the weak East Asian summer monsoon in the model climate (see Fig. 10 and Hu et al. 2000).

To assess the model skill to simulate local temperature variability, the model STD is calculated by averaging ten STD patterns of ‘masked’ 100-year periods. The result is compared with the STD of the 100-year (1901-2000) HadCRUT observations. To remove climate signals from external forcing in the simplest way, linear trends are removed locally before calculating standard deviations of the model and observations (Stouffer et al. 2000). More than 10 months for annual mean and more than 30 years for interannual STD are required to obtain non-missing observations. Figure 6 shows variability patterns of annual mean T2m. The observed pattern shows dominant variability (> 1.0°C) on the continents north of 60°N and large variability (> 0.5°C) in the NH mid latitude (Fig. 6b). Patches of large STD also occur over the North Pacific and the North Atlantic, as well as over the equatorial eastern Pacific (> 0.5°C). Overall, the model captures the observed features of temperature variability quite well (Fig. 6a), but the logarithm of the ratio of model and observational variability (Fig. 6c) shows that the model has larger variability than observed in the North Pacific, North Atlantic, and Himalayan Mountains, and smaller variability over the rest of the ocean, especially in the tropics. The decadal variability of surface temperatures computed from 5-year-mean time series (Fig. 7b) shows characteristics similar to those described above. More than 3-year annual means are considered for non-missing 5-year means. Larger variability appears in high latitude continents, the central North Pacific, North Atlantic, and equatorial Pacific. The model simulates T2m variability over NH continents very well, but overestimates the variability in the North Pacific and North

Atlantic while the T2m variability in the tropical oceans is underestimated (Fig. 7c).

3.2 Precipitation

Figure 8 shows time series of ANN, DJF, and JJA global mean PCP. As in the time series of T2m in Figure 1, there is little climate drift in the simulated PCP. ECHO-G simulates a little bit more PCP than seen in the observations: Climatological values of the global mean PCP rate in the model are 2.80, 2.74, and 2.86 mm/day for ANN, DJF, and JJA mean, respectively, which are 0.10-0.12 mm/day larger than observational values of 2.68, 2.64, and 2.78 mm/day estimated from the 20-year mean (1979-1998) of CMAP data (Xie and Arkin 1997). The amplitude of the model PCP seasonal cycle (JJA minus DJF) is 0.12 mm/day while the observed value is 0.14 mm/day.

A comparison of the simulated geographical distribution of DJF PCP with CMAP observations is shown in Figure 9. The meridional distribution of zonal mean PCP are fairly well simulated by the model with a small wet bias over the NH mid latitude and a dry bias near 40°S. The wet bias in the mid-latitude of the winter hemisphere is a common problem in CMIP AOGCMs (Lambert and Boer 2001). The structure of the Inter-Tropical Convergence Zone (ITCZ), the South Pacific Convergence Zone (SPCZ), and the dry tongue in the equatorial Pacific are well captured by the model although the amplitudes of the ITCZ and SPCZ are a little bit smaller than observed. Biases as e.g. the positive deviations over South Africa, Australia, and the western Indian Ocean are of the same order as those in ECHAM4 integrations with prescribed observed SST (Roeckner et al. 1996a). PCP in JJA is shown in Figure 10. As in DJF, the overall pattern is well simulated by the model including the ITCZ and SPCZ structure. However, negative biases dominate in the Indian and Asian monsoon region and the eastern tropical Pacific. A maximum PCP appears over the Indian Ocean in the model, while it is positioned along the west coast of India and over the Bay of Bengal in the observations. This shortcoming also appeared in ECHAM4 stand-alone simulations (Roeckner et al. 1996a), indicating that the monsoon simulation of the model is not affected by the coupling system applied here. In contrast to the DJF result, a wet bias is seen in JJA PCP over the SH mid-latitudes. The zonal mean JJA PCP represents a good performance except for the wet bias in the SH mid-latitude.

The local temporal variability of annual mean PCP in the model is compared with 20-year CMAP observations in Figure 11. The model STD is evaluated at each grid point by averaging 50 standard deviations calculated from 20-year subperiods. As in the case of T2m variability in Figure 6 and Figure 7, the long-term linear trends are removed locally in advance for both simulations and observations. The observed pattern of interannual variability of precipitation (Fig. 11b) reveals dominant variability (> 1.0 mm/day) in a zonal

band of the tropical Pacific and eastern Indian Ocean with a maximum larger than 2 mm/day in the equatorial central Pacific. The meridional extent of larger variability (> 0.5 mm/day) is from 30ºS in the central Pacific to 30ºN in the western Pacific. The equatorial Atlantic also shows larger variability. The overall pattern of the PCP variability is captured reasonably well by the model. However, its amplitude is lower than the observed in the eastern and western equatorial Pacific, South America, northwestern Pacific, and equatorial western Africa. It is noted that the spatial pattern of the precipitation variability in the model and observations is dominated by ENSO-related fluctuations on the time scale considered here. The decadal variability cannot be studied because of the short length of the observational period of 20 years.

3.3 Mean sea level pressure

Figure 12 shows geographical and zonal mean patterns of DJF MSLP of ECHO-G CTL and observations (1961-1990 mean of NCEP/NCAR reanalysis), as well as their differences. The comparison of zonal mean reveals overall good consistency between the model and observation such as the tropical low, subtropical highs, and high-latitude lows. The zonal mean pattern of the model bias reveals that the subtropical highs in NH and the high-latitude lows have positive pressure biases. The amplitude of the model bias is less than 5 hPa except for the SO and Antarctic regions. When compared with other AOGCMs, ECHO-G exhibits a relatively good skill in simulating the zonal mean MSLP, especially at the low and mid-latitudes (Lambert and Boer 2001). The overall geographical patterns of DJF mean MSLP are well represented in the model control simulation including the position and amplitude of the main high and low pressure systems in NH. The Aleutian Low and the Icelandic Low are well reproduced except that the center of the Aleutian Low is located more eastward in the model climate than in the observations. The Siberian High in the model is stronger especially in the northern part of Siberia. The Azores High in the model is stronger by more than 10 hPa and has a more eastward position. On the other hand, the subtropical highs in the SH mid-latitude have weak negative pressure biases while the Antarctic region has a strong positive bias. The stand-alone version of ECHAM4 shows very similar patterns of model bias in DJF MSLP (Roeckner et al. 1996a), which indicates that the coupled system does not change significantly the climate of the atmospheric surface pressure as is the case for PCP.

The comparison of JJA MSLP is shown in Figure 13. The model climate captures the overall pattern of observations quite well except for higher latitude regions in both hemispheres. The strong biases south of 60ºS may be artifacts caused by large errors in the reanalysis MSLP in this region (Marshall 2003; Marshall and Harangozo 2000). The

subtropical highs in the North Pacific and North Atlantic are simulated well both in position and strength. The Eurasian continental low in the model has a positive bias or weaker strength than observed which may be related to the cold bias there and the weak summer monsoon (see above). The southern part of North America has a negative bias. Subtropical highs on the SH are well positioned, but they are a little bit weaker than observed. A large negative bias appears in the SH mid-latitudes.

In order to assess the model skill in simulating the interannual variability, the STD of annual mean MSLP is calculated at each grid point and its horizontal distribution is shown in Figure 14. The STD of the observed MSLP is evaluated from the 40 year period (1961-2000) of NCEP/NCAR reanalysis while the STD of model climate is obtained by taking the mean of 25 standard deviations for 40-year subsections of the 1000-year CTL. The linear trends in the 40-year period are removed for both model data and observations before calculating the STDs. The observed pattern of MSLP variability displays large variability (> 1.5 hPa) in the North Pacific, North Atlantic, and polar regions in both hemispheres which appears to be related to the North Pacific Oscillation (NPO), NAO, Arctic Oscillation (AO), and Antarctic Oscillation (AAO) or hemispheric annular modes (Rogers 1990; Thompson and Wallace 1998, 2000, 2001) (see also Figure 25 for DJFM MSLP variability in the NH extratropics). It is also observed that generally the amplitude of MSLP variability is larger at higher than at lower latitude and over the oceans than over land. Figure 14 shows that ECHO-G is able to reproduce the overall pattern of the observed MSLP variability but mostly with smaller amplitudes than observed. Exceptions are a relatively large model variability over the equatorial central Pacific (> 0.5 hPa), which might be related to the strong and regular El Niño-like variability in the model (see below), and over the northern North Pacific.

4. The El Niño–Southern Oscillation

4.1 ENSO amplitude and frequency

Figure 15 shows the monthly time series of the NINO3 index calculated from the GISST observations (1903-1994) and the first 92 years of ECHO-G CTL. The NINO3 index is defined as the area-mean SST anomaly in the NINO3 domain (150-90°W and 5°S-5°N). The SST anomalies are evaluated relative to the 1961-1990 monthly means for the observations and to the whole 1000-year monthly means for the model. The amplitudes of the NINO3 index in the model are larger than the observed. The STD of the linearly detrended NINO3 index is 0.64°C for the observations (1905-1994) and 1.15°C for the model ranging from 0.93 to 1.23°C for 11 90-year subsections of the 1000-year simulation period.

The second feature of the simulated ENSO in the time series of Figure 15 is that large positive/negative anomaly events (El Niño/La Niña) develop more frequently in the model than in the observations. This too frequent ENSO phenomenon in the model can be more clearly seen in the analysis of power spectrum shown in Figure 16. As for the global mean temperature in Figure 3, the spectrum of the NINO3 index in the model is calculated by averaging 11 spectra of the NINO3 index from 90-year subsections of the 1000-year CTL, while the observed spectrum is obtained from the 90-year period of 1905-1994. The mean and range (maximum and minimum) of the model spectrum are depicted as a thick line and shading, respectively. The model spectrum of NINO3 index exhibits a dominant 2-year peak while the observational NINO3 index has a broader spectral peak near 3-7 years. This problem is known to occur in AOGCMs with ECHAM4 as the atmospheric component. Guilyardi et al. (2003) discussed this problem by comparing the El Niño characteristics in AOGCMs with the same AGCM (ECHAM4-T30 or T42) but different ocean GCMs (ORCA, OPA, or OPYC3) and proposed that a stronger than observed Walker circulation (or stronger trade winds) might be an important factor to cause such a high-frequency ENSO (Fedorov and Philander 2000). Guilyardi et al. (2004) presented a new modular approach to investigate the respective role of the atmosphere and ocean in El Niño simulations of AOGCMs and found a dominant role of the atmospheric resolution in controlling the El Niño frequency, that is, the higher the model resolution the lower the El Niño frequency. Latif et al. (2001) found too regular occurrences of ENSO in many AOGCMs and pointed out that its cause is still unclear and other factors can play a role such as the noise level of the atmospheric component (Eckert and Latif, 1997; Blanke et al. 1997) or the phase locking of ENSO to the annual cycle (Chang et al. 1994).

Figure 16 also indicates that the model has more energy at time scales shorter than 3 years and less energy at the time scale of 4-7 years. This is statistically significant at the 94% confidence level (ln 2 / 11 sections) following the formula by Gillett et al. (2000). The reason for this is not known and needs further analysis.

4.2 ENSO structure in the equatorial Pacific

a. SST climatology and variability

Figure 17 shows annual mean SST and the variability of SST anomalies at the equatorial Pacific (between 2°S-2°N) for ECHO-G CTL and the GISST observations. The model is capable of simulating the SST climatology. The warm pool in the western Pacific, the cold tongue in the east Pacific, and zonal SST gradient (with a magnitude of about 0.4°C per 10° longitude) in the central part of the basin are realistically simulated. This is consistent with previous results that generally flux adjusted models have a better skill in simulating the SST

climate and gradients, although the flux correction does not guarantee a better simulation (Latif et al. 2001; Davey et al. 2002; AchutaRao and Sperber 2002). The warm SST bias of about 1.5°C that appears near the eastern boundary in Figure 17a is a common error in many AOGCMs typically linked to problems in simulating stratus clouds and coastal upwelling (Mechoso et al. 1995; Latif et al. 2001; Davey et al. 2002; AchutaRao and Sperber 2002).

The STDs of the observed and simulated SST shown in Figure 17b are calculated after removing the seasonal cycle. The observed profile shows small variability of 0.4°C in the western Pacific and starts to increase at 160°E to a maximum value of 0.9°C at 105°W. ECHO-G also has smaller values in the western part and larger in the eastern part, but overestimate the variability in the central and eastern Pacific with maximum 2.0°C near 125°W. AchutaRao and Sperber (2002) reported that most (13 from 17) AOGCMs underestimate the SST variability in the eastern Pacific except for four models (ECHAM4/OPYC3, HadCM3, DOE-PCM, and CERFACS) of which ECHAM4/OPYC3 is the only model with flux corrections. Considering that ECHO-G exhibits features very close to those of ECHAM4/OPYC3 in the simulation of SST variability, namely that both models use only annual mean flux corrections for heat and moisture and no flux correction for momentum, there might be a potential influence of the flux correction method on the strength of simulated SST variability.

b. Seasonal cycle of SST, zonal wind stress, and ITCZ

The seasonal cycle of the equatorial Pacific SST involves complex dynamic and physical interactions between atmosphere, ocean, and land, and therefore provides a criterion for the overall skill of coupled models in the tropics (Latif et al. 2001). Figure 18 shows the annual cycle of SST about the annual mean depicted in Figure 17 at the equatorial Pacific for ECHO-G CTL and the GISST observations. The observed annual cycle is represented by three characteristics. The first is an annual harmonic variation with large amplitude in the eastern Pacific with a range of about 4.5°C, a maximum in March (> +2.5°C), and a minimum (~ -2°C) in September. The second is a semiannual harmonic with smaller amplitude in the western Pacific with two positive phases in April-May and October-November and two negative phases in June-September and December-February. The third is a westward propagation of SST in the central and eastern Pacific. ECHO-G captures these three observed features reasonably well except that the range of the seasonal cycle is smaller (about 3°C) in the eastern Pacific and the minimum SST appears later in November-December and positioned about 20° westward compared with the observed. According to previous work, many AOGCMs simulate too weak annual cycles in the eastern Pacific (Mechoso et al. 1995; Latif et al. 2001). A high resolution of the ocean component is a

necessary (but not sufficient) condition for a good simulation of the SST annual cycle, and flux corrected models are generally able to simulate the amplitude and phase of the seasonal cycle better; although there are exceptions (AchutaRao and Sperber 2002). Since ECHO-G is categorized into the AOGCMs with high resolution ocean model (higher than one degree) and flux correction (annual mean only), the good performance of ECHO-G in the simulation of SST seasonal cycle corroborates these previous findings.

Figure 19 shows the annual mean climatology and the seasonal cycle of zonal wind stress in the equatorial Pacific for ECHO-G CTL and the SOC observations. The SOC climatology is an average for 1980-1993 (Josey et al. 1999) whereas ECHO-G climatology is for the 1000 years along with 14-year averages for 71 subsections. The overall pattern of zonal wind stress including the location of maximum values near 150°W are well reproduced by ECHO-G but the simulated amplitude is larger (0.075 N/m^2) than the observational value (0.05 N/m^2). Davey et al. (2002) showed that AOGCMs without flux adjustment tend to have too weak easterly wind in the central equatorial Pacific and that flux adjusted AOGCMs have quite similar gradients of zonal wind stress though the maximum strength ranges from 0.04 to 0.08 N/m^2. When compared with the 23 AOGCMs used in Davey et al. (2002), ECHO-G simulates the strongest easterlies in the equatorial Pacific along with ECHAM4/OPYC3 (0.08 N/m^2). This suggests that the atmospheric component plays a crucial role in setting up the zonal wind stress in the equatorial Pacific in coupled models. In addition, as discussed above, the strong zonal wind stress (strong Walker circulation) might be related to the frequent and regular ENSO in ECHO-G (see section 4.1 above).

The lower panel of Figure 19 shows the observed and simulated seasonal variation of the zonal wind stress. The observations exhibit a clear westward propagation of zonal wind stress: a positive zonal wind deviation (weaker easterlies) in the eastern Pacific in February-March moves to the western Pacific by October-November and a negative deviation (stronger easterlies) in 180-150°W in January moves to the western boundary by August-September. ECHO-G is not capable of simulating the annual cycle or propagation of zonal wind stress. A semi-annual cycle dominates in the western Pacific with stronger amplitudes (maximum larger than 20 N/m^2) than observed (~10 N/m^2). The problem of the erroneous semi-annual component in the zonal wind annual cycle is found in several AOGCMs (Davey et al. 2002).

Mechoso et al. (1995) showed that many AOGCMs simulate too narrow, strong, and westward extended cold tongues and too warm SSTs south of the equator in the eastern Pacific region and that this is in some models accompanied by a double ITCZ or a migrating ITCZ across the equator in the eastern Pacific. When SST patterns in the tropical Pacific

simulated in ECHO-G are compared with GISST observations for each season (Fig. 20), it is found that ECHO-G can simulate seasonal SST patterns very realistically including the zonal and meridional extent of the warm pool and the cold tongue. There is a good consistency between model and observation: almost no cold tongue in MAM, strong southeast cold tongue in SON extending westward to the date line, and the largest warm pool in SON. However, the cold tongue and associated warm tongue south of the equator are narrower meridionally in ECHO-G than in the GISST data. In order to see the behavior of the ITCZ in ECHO-G CTL, the observed and simulated seasonal cycles of precipitation over the eastern Pacific (averaged between 150-100°W) against latitude are compared in Figure 21 (also see Fig. 9 and Fig. 10). The observations reveal a single ITCZ located persistently between 5°N and 15°N with maximum values (~10 mm/day) near 10°N in June-August. ECHO-G catches the observed single ITCZ reasonably well. It shows no migration across the equator, though a weak double ITCZ can be found in February-March. However, the simulated amplitude of the ITCZ is weaker with maximum values of ~6 mm/day, and the maximum PCP rate appears in October-November, later than in the observations. This relatively good simulation of the ITCZ and SPCZ in ECHO-G can be attributed to the ECHAM4 physics, i.e. the convection scheme based on the convective instability and buoyancy closure as discussed in Roeckner et al. (1996b) (see also Frey et al. 1997).

c. ENSO phase-locking to the annual cycle

The interannual STD of SST anomalies in the NINO3 region for each calendar month is shown in Figure 22. It demonstrates the phase-locking of ENSO to the annual cycle. The observed standard deviation exhibits a maximum in December (~0.9°C) and a minimum in April (~0.5°C), which means that peak ENSO events occur in the NH winter. ECHO-G captures the pronounced winter maximum and spring minimum, but the maximum is reached too early in July with overestimated amplitude and is maintained till next January. AchutaRao and Sperber (2002) showed that most AOGCMs taking part in CMIP1 have weak variability and no seasonal peak at all, and that only three models (ECHAM4/OPYC3, HadCM2, and HadCM3) simulate reasonably well the phase and amplitude of the interannual variability of ENSO. Since there is no systematic relation between the simulation of a realistic SST annual cycle and the simulation of ENSO phase-locking to the annual cycle (Latif et al. 2001), ECHO-G is evaluated to have a good skill in simulating both the SST annual cycle (Fig. 18) and the ENSO seasonal cycle phase-locking (Fig. 22) compared to other models.

4.3 El Niño response

In this section, simulated and observed atmospheric responses to ENSO are compared with the help of correlation and regression patterns for T2m, PCP, and MSLP with the NINO3 index for the DJF season when the observed El Niño reaches its maximum amplitude (Fig. 22). Figure 23 shows the spatial distribution of correlation coefficients, while the corresponding regression maps are given in Figure 24. HadCRUT are used as observations for the period of 1903-1994, and grid points where the number of observations is less than 20 in DJF are treated as missing points. The observational correlations of T2m with the El Niño index are significantly positive over the tropical central and eastern Pacific, northern North America, the west coast of North and South America, the Indian Ocean and southern Africa while significant negative values appear in the central North Pacific and southern North America. For the 999 DJF means of ECHO-G, the threshold for significant correlation coefficients is 0.06 [0.08] at the 10% [5%] significance level (two-tailed t test). The ECHO-G correlation pattern (Fig. 23a) captures the observed features of the ENSO-related T2m pattern well, except that the region with positive values in the central equatorial Pacific extends more to the west and the correlation is higher over northern North America, northern South America, and the Indian Ocean. Also ECHO-G does not simulate realistically the observed symmetry of T2m response to ENSO about the equatorial Pacific (Trenberth and Caron, 2000). The regression map of T2m with the NINO3 index (Fig. 24a,b) shows that, during El Niño events, the region with anomalously warm T2m in the tropical Pacific in ECHO-G is more confined to the equator and extends more eastward towards Brazil. The region with positive correlations over northern North America is shifted northwestward compared to the observations with a maximum near Alaska. Overall, however, scales and patterns are well reproduced.

The observed correlation pattern of DJF PCP with the NINO3 index (Fig. 23d) is more localized or noisier than the T2m and MSLP patterns. Since only 15 DJF (1979/80-1993/94) CMAP data are used to calculate the correlation coefficients, a statistically significant correlation is obtained only above 0.51 [0.64] at the 10% [5%] significance level. During El Niños, precipitation above average occurs in the tropical central and eastern Pacific, southeastern Pacific, southeastern North America, and at the west coast of North America, while it is statistically significant below average in the equatorial western Pacific, the tropical Pacific north and south of the equatorial larger precipitation area, northeastern Brazil, and southeastern Africa. Even if very short periods of observations are taken, the overall features are very similar to those shown previously by Ropelewski and Halpert (1987) and by Trenberth and Caron (2000). ENSO-related precipitation anomalies in ECHO-G CTL (Fig. 23c) exhibit a very realistic correlation pattern compared with the observed, especially the merging of ITCZ and SPCZ into a huge convective system centered at the

equator in the mature phase of ENSO (Roeckner et al. 1996b; Trenberth and Caron 2000) is well reproduced. However, positive correlations in the equatorial central Pacific extend more westward and southeastward off the west coast of South America, and the negative correlations in the tropical Pacific of both hemispheres are more trapped near the equator than the observed (compare also the regression maps in Fig. 24c, d). This is closely linked with the problem of T2m response (Fig. 23a, b). Precipitation regressions in Figure 24c,d show that the amplitudes of precipitation changes related to ENSO are reasonable in ECHO-G CTL.

In the observed correlation of MSLP with the NINO3 index (Fig. 23f), the apparent response of atmospheric mass to ENSO is characterized by an oscillation between two centers of action, the Indonesian center and tropical Pacific center. The statistically significant correlation is 0.33 [0.42] at the 10% [5%] significance level for the 36 DJFs of the MSLP fields of NCEP/NCAR reanalysis from 1958/59-1993/94. The Indonesian center of action extends into Africa and the tropical Atlantic, while the tropical Pacific center of action extends northward into the North Pacific (Fig. 23f). The regression map for the observed MSLP shows larger variation of ENSO-related MSLP over the North Pacific and South Pacific at high latitudes than in the tropics (Fig. 24f). The MSLP response to ENSO in ECHO-G CTL resembles the observational field nicely (Fig. 23e). Correlation fields in the model display a good location of the two centers of action although shifted westward about 10-20°. The correlations in the model are stronger than observed in the central equatorial Pacific (and more confined to the equator similarly to the patterns of T2m and PCP), over Indonesia, the Indian Ocean, and the west coast of North America, whereas they are weaker over central Africa and the tropical Atlantic. Regression maps of MSLP in Figure 24e show that the magnitude of the MSLP response to ENSO in the model is reasonable, including the deepening of the Aleutian Low and its southeastward displacement (van Loon and Madden 1981; Roeckner et al. 1996b). However, the negative anomaly in the North Pacific is stronger and broader and the positive anomaly in the western tropical Pacific does not extend sufficiently northeastward in ECHO-G.

In summary, the atmospheric response to ENSO in ECHO-G CTL indicates that ECHO-G can be classified into the category Group I defined by AchutaRao and Sperber (2002), containing the models which are most consistent with observations. The AOGCMs in Group I (ECHAM4/OPYC3, HadCM2, CERFACS, DOE-PCM, and HadCM3) have a well-defined Walker circulations, enhanced warming extending from the tropical central Pacific to the west coast of South America, and associated rainfall in the tropical Pacific (AchutaRao and Sperber 2002). While ECHAM4/OPYC3 and CERFACS simulate a warming displaced further to the northeast over Hudson Bay and Greenland and the other

three AOGCMs in Group I have a cooling over North America (AchutaRao and Sperber 2002), ECHO-G simulates the warming over North America quite well (Fig. 24a). Therefore, ECHO-G can be considered to have a good skill in simulating the atmospheric response to ENSO compared with other AOGCMs.

5. The North Atlantic Oscillation

5.1 Wintertime MSLP variability in the NH

The NAO is one of the major internal climate variability signals in the NH extratropics with monthly to decadal time scales, and exerts a strong influence on the climate of the Euro-Atlantic and Pacific regions (Thompson and Wallace 2001). Various methods have been proposed to define a NAO index, e.g. the pressure difference between stations on the Azores and Iceland (Rogers 1984; Hurrell 1995; Jones et al. 1997), the leading principal component (PC) time series of NH MSLP field (Rogers 1990; Thompson and Wallace 2000, 2001), or the first PC of time series of intensity and latitudinal position of the Azores High (AH) and the Icelandic Low (IL) (Glowienka-Hense 1990; Paeth et al. 1999). In this section, we compare the simulated NAO with the observed using the station-based NAO index (Gibraltar minus Iceland DJFM mean MSLP) of Jones et al. (1997), and, in addition, compare the station-based simulated NAO index with the PC-based one. The spatial structure is examined by comparing local patterns of observed and simulated interannual variability of MSLP.

Figure 25 shows maps of interannual variability or STD of DFJM MSLP in the NH extratropics (20-90°N) for ECHO-G CTL and NCEP/NCAR reanalyses. In contrast to Figure 14 (global map of STD of annual mean MSLP) the linear trend is not removed in order to retain the decadal variability. The observed pattern in Figure 25b exhibits two centers of action with large variability (> 5 hPa) situated over the northern North Atlantic and the North Pacific. The North Atlantic center broadly extends to the Arctic Ocean. The simulated MSLP variability reproduces well the observed location and strength of the two centers, but the simulated variability in the Atlantic sector is somehow (about 1 hPa) weaker than the observed (Fig. 25a). As shown earlier in Figure 12a,b, the wintertime mean MSLP pattern is reasonably well simulated in ECHO-G CTL including the position of IL although the simulated AH is stronger and shifted towards the east.

The eigenvector pattern and time series of the leading PC of DJFM MSLP in the NH extratropics for the NCEP/NCAR reanalyses (1958/59-2000/01, 43 DJFMs) are shown in Figure 26. The time series of the station-based NAO index (Jones et al. 1997) is drawn together with the PC time series for better comparison. The very high correlation (0.86)

between the PC time series and the NAO index indicates that the leading PC mode of MSLP corresponds to the NAO mode. It explains 34.0% of DJFM MSLP interannual variability in the NH extratropics. The observed PC spatial pattern is characterized by a dominant north-south dipole structure in the North Atlantic sector. The dipole represents the well-known strengthening [weakening] of AH and IL (or pressure gradient and zonal wind advection from the Atlantic into western Europe) in the positive [negative] NAO phase. It is notable that there is no Pacific center of action in the observations used here (Fig. 26a), differently from the leading Empirical Orthogonal Function (EOF) mode of Thompson and Wallace (1998) where an additional center of action over the North Pacific is found (see Figure 1 of Thompson and Wallace 1998). However, Thompson and Wallace (1998) could obtain the Pacific center of action for the last 30 years (1968-1997) only after removing the linear trend for each grid point because the MSLP decreasing trend over the North Pacific for this period is strong enough to cancel the center of action over the North Pacific in their EOF of wintertime mean MSLP.

Figure 27 shows the simulated leading PC of wintertime MSLP. The percentage of explained variance is 30.5%, close to the observed 34.0%. This mode represents NAO variability in ECHO-G CTL since the PC time series is positively correlated (0.76) with the station-based NAO index. The spatial pattern of the corresponding eigenvector shows a dipole structure in the Atlantic sector similar to the observed, but its amplitude is about half of the observed value only. The main weakness of the simulated PC pattern is that too strong variability appears in the North Pacific which is not found in the observational PC pattern (Fig. 26a). Also, too strong negative correlations (-0.29, significant at 99% confidence level) between the DJFM NINO3 and NAO indices is found in the model simulations while there is almost no correlation observed, e.g. -0.05 for 92-DJFM observations (1903-1994). Stephenson and Pavan (2003) also addressed a very low observational correlation (+0.02) between the DJF NINO3 and NAO indices (1900-1991). The dominant North Pacific variability might be highly influenced by the strong and regular ENSO variability in the ECHO-G CTL (see section 4) as was found in other AOGCMs such as ECHAM3/LSG (Timmermann et al. 1998), HadCM2 (Osborn et al. 1999), HadCM3 (Collins et al. 2001), ECHAM4/OPYC3, NCAR CSM, and CCSR (Stephenson and Pavan 2003). Stephenson and Pavan (2003) speculated that an overly strong teleconnection between the tropics and the extra-tropics might cause the problem. The 5-year running mean time series of the leading PC of the model MSLP reveals long-term variations with decadal to centennial time scales (Fig. 27b), trends of which will be compared with the observed change of the NAO index (Fig. 26b) below in the context of the detection of human impacts.

5.2 Power spectrum and trend analysis of the NAO index

Figure 28 shows the time series of station-based NAO index anomalies for 999-DJFM ECHO-G CTL and 177-DJFM observations (1825/26-2001/02). The DJFM MSLP difference (Gibraltar minus Iceland, Jones et al. 1997) is defined as the NAO index for both datasets. There is almost no long-term trend in the model NAO (-0.022 hPa/century) whereas the observations have a weak increasing trend of 0.11 hPa/century. The observed magnitude of the NAO trend seems to be within the model internal variability. When the amplitude of the NAO variability is estimated from standard deviations in the detrended time series, the model NAO amplitude (~5.5 hPa) is somehow smaller than the observed (~6.4 hPa). Distinct decadal variability can be seen in both datasets.

Power spectra of the simulated and observed linearly detrended NAO index are shown in Figure 29. The model period of 999 DJFMs is divided into five 177-year subsections and the power spectra obtained from the five subsections are averaged to define the mean spectrum of the model data. The observed spectrum indicates near-white behavior with no significant spectral peaks meaning that there is no periodic signal in the observed NAO. Osborn et al. (1999) pointed out that the observed spectral shape for NAO varies highly between definitions. The NAO index of Jones et al. (1997), used in this study, exhibits a spectrum close to white noise while the Azores minus Iceland version produce a redder spectrum (see Hurrell and van Loon, 1997; Wunsch 1999; Stephenson et al. 2000). The NAO spectrum simulated by ECHO-G exhibits a very similar flat behavior with no preferred time scale although there exist a couple of spectral differences for long-term scales (> 40 years) and near 8 year periods between the simulated and observed NAO variability.

Using the simple detection method defined by Collins et al. (2001), as in section 3.1 for T2m, the observed NAO index trend is compared with the simulated for different time scales in Table 4. The number of simulated NAO trends larger than the observed is counted and its relative occurrence is given by dividing it by the total number of trends for each period. The observed trend in the NAO index is largest (0.25 hPa/year) in the recent 40-year period of 1960-1999 and the second largest trend appears as a 50-year trend (0.18 hPa/year) in 1950-1999. Such a large increase cannot be found in the model control run and the 60-year observed trend also occurs very infrequently (~0.3% chance). On the other hand, the observed trend for the recent 10-30 year period is simulated with a chance of more than 1% by the model. This result is in accordance with previous analyses of multi-century control runs with HadCM2 (Osborn et al. 1999) and HadCM3 (Collins et al. 2001).

Some studies provide statistical evidence that the recent NAO change might include anthropogenic effects by comparing the observed NAO trend with those from climate change simulations forced with increasing greenhouse gases (e.g. Shindell et al.

1999; Paeth et al. 1999). Other studies suggested an important role of the tropical oceans (e.g. Hoerling et al. 2001) or of the Atlantic Ocean (e.g. Rodwell et al. 1999; Robertson et al. 2000; Paeth et al. 2003) in the decadal variations of the observed NAO. However, the question whether the observed NAO trend can be explained by natural variability or is a response to increasing concentrations of anthropogenic greenhouse-gases is still largely controversial because the NAO response to greenhouse warming is different from model to model (see e.g. Osborn et al. (1999) for the HadCM2 response, Paeth et al. (1999) for ECHAM3/LSG and ECHAM4/OPYC3, and Fyfe et al. (1999) for CCCma GCM), and the observed oceanic forcing has partly an effect of greenhouse warming inside (Bretherton and Battisti 2000).

5.3 NAO related patterns of atmospheric variables

Figure 30 and 31 show the maps of correlation and regression patterns of DJFM mean T2m, PCP, and MSLP with the NAO index shown in Figure 28 for the observations and the model control simulation. HadCRUT, CRU-PCP, and NCEP/NCAR reanalysis MSLP are used for observational data (Table 2). In the observational data sets of HadCRUT and CRU-PCP, grid points where the number of DJFM mean observations is less than 20 are treated as missing points. The regression coefficients indicate the atmospheric response to one STD of the NAO index (Hurrell 1996; Osborn et al. 1999). The observed NAO-related T2m correlation pattern in Figure 30b is characterized by quadrupole structure over Atlantic Sector (Hurrell and van Loon 1997; Osborn et al. 1999; Stephenson and Pavan 2003). There are two regions with strong positive correlations (> 0.3), the first centered over Scandinavia and reaching downstream into northern Russia, and the second over southeast North America, as well as two regions with negative correlations (< -0.3), one centered over the Labrador Sea and the other over northern Africa (Fig. 30b). The model captures the observed quadruple pattern realistically including the location of the above mentioned four centers, but the simulated correlation is lower over the Eurasian sector, especially over northern Russia, and the positive correlation of southeast North America is shifted eastward relative to the observed (Fig. 30a). An observed warm response larger than 1°C/STD to a positive NAO index exists over northeastern Europe (Fig. 31b). The model regression map reproduces the observed quite well with similar amplitude, but the warming over northern Russia is smaller in the simulations (Fig. 31a). ECHO-G also shows a weakness by simulating a broad cooling response over northern Canada that extends further into Alaska than found in the observations. Comparing the T2m correlation map of ECHO-G (Fig. 30a) with the leading eigenvectors of the T2m correlation matrix for 17 AOGCMs shown by Stephenson and Pavan (2003), ECHO-G model shows a good skill in the simulation of the T2m quadruple

pattern over the Atlantic.

The observed correlation of PCP with the NAO index exhibits the well-known pattern of dry conditions over southern Europe and the Mediterranean and wetter-than-normal conditions over northern Europe and Scandinavia (Hurrell and van Loon 1997) during positive NAO phases (Fig. 30d). ECHO-G reproduces the observed pattern of NAO-related PCP over Europe (Fig. 30c). However, the simulated dry area over southern Europe extends further eastward. The other observed features involve positive correlations over southern North America and weak negative correlations over northern North America (Fig. 30d). ECHO-G cannot simulate the North American pattern correctly (Fig. 30c). The regression maps of precipitation are drawn with percentage change relative to the 30-year (1961-1990) climate for observation and the 1000-year mean for the model data (Fig. 31c, d). The observed magnitude of precipitation change associated with the NAO is well simulated by ECHO-G over Europe.

The observed correlation pattern of MSLP with the NAO index exhibits a distinct dipole structure over the Atlantic with little correlation over the Pacific. A positive center of correlation above 0.8 is located over Gibraltar and a negative one below -0.8 over Iceland (Fig. 30f). ECHO-G reproduces the observed dipole pattern of MSLP correlation realistically except for the fact that the simulated correlations are weaker than the observed, especially in the positive center over Gibraltar (compare contour lines +0.6) and that the positive center is positioned further westward than the observed (Fig. 30e). The most evident differences between the simulated MSLP correlation map and the observed are the positive correlations larger than 0.4 south of the Aleutian Low which extend westward over Japan and the negative correlations stronger than 0.2 over the Indian Ocean and Indonesia, the first feature being absent while the second has a reversed sign in the observations (Fig. 30e). The regression maps of MSLP (Fig. 31e,f) support these results. When the NAO index is higher than normal by one STD, the observed maximum (> +2.5 hPa/STD) of MSLP change is located over the west Iberian Peninsula, northwest of the correlation maximum, and a minimum (< -5 hPa/STD) appears over Iceland identical to the correlation minimum (Fig. 31f). ECHO-G CTL captures the observed regression pattern but underestimates the amplitude by 1-1.5 hPa/STD over the two centers of action and over Siberia while it produces a too large MSLP response over the North Pacific during positive phases of the NAO. The additional North Pacific center and therefore more zonally symmetric pattern in the model represents a closer resemblance to the observed AO (Thompson and Wallace 1998). This may be associated with a closer link between the NAO and the ENSO, i.e. an overestimated Atlantic-Pacific teleconnection, which is an error seen in many AOGCMs as discussed in section 5.1. The enhanced Atlantic-Pacific teleconnection in ECHO-G CTL can

be easily seen if one compares the correlation maps for the NAO and NINO3 indices. In the tropical Pacific, NAO correlation patterns in Figure 30a,c,e are very similar with reverse signs to those of NINO3 in Figure 23a,c,e.

6. Summary and discussion

This paper describes the climate and internal variability of a 1000-year control simulation (CTL) with the coupled climate model ECHO-G using present constant values of well-mixed greenhouse gases and no external forcing. It provides a background for future scenario simulations. The skill of ECHO-G in reproducing the mean climate and variability is compared with that of other AOGCMs. ECHO-G consists of the atmospheric component ECHAM4 and the oceanic component HOPE-G, and includes a dynamic and thermodynamic sea-ice model. Flux corrections are applied for annual-mean heat and freshwater only, with zero global mean, and there is no correction in high latitudes poleward of the climatological AMIP ice edge. The model simulates almost no climate drift.

The internal variability of three surface variables (T2m, PCP, and MSLP) and the two dominant signals of natural climate variability (ENSO and NAO) are examined. The ECHO-G control experiment shows an overall good skill in simulating the seasonal mean climatology and the interannual variability of T2m, PCP, and MSLP. Biases in the model climate of the three variables are very similar to those of ECHAM4 stand-alone integrations (Roeckner et al. 1996b) except for the JJA T2m in the Arctic region which may be related to the partial sea ice cover used in the coupled model in contrast to the stand-alone integrations (see Grötzner et al. 1996).

Local temporal variability of the T2m at interannual to interdecadal time scales are reproduced realistically over the NH continents, but it is overestimated over the North Pacific and North Atlantic while underestimated over the tropical oceans. ECHO-G locates the ITCZ and SPCZ realistically although there are biases in amplitudes. The PCP associated with the Indian and East Asian summer monsoon is underestimated, which is speculated to be linked with the cold bias in the Asian continental T2m (i.e. weak land-sea temperature contrast) and with the weakly simulated Eurasian continental low in the model. The observed large variability of PCP in the tropical Pacific is well captured by the model but its amplitude is underestimated whereas the spatial pattern of the MSLP STD exhibits weaker variability over Africa and the tropical western Pacific than the observations.

It is shown that the ENSO-like variability in the model has stronger than observed amplitudes and is too frequent and regular. This is probably the reason for a too strong 2-year peak in the simulated global mean T2m energy spectrum and the underestimated energy

at periods of 3-9 years. The cause of the high frequent ENSO is still unclear, but our model result corroborates previous suggestions that the horizontal resolution of the atmospheric model plays a dominant role (Guilyardi et al. 2004) as well as the Walker circulation (Guilyardi et al. 2003), and noise levels (Latif et al. 2001). ECHO-G CTL shows reasonable skill in simulating ENSO structures such as the tropical Pacific SST climate and its seasonal cycle, the warm pool and cold tongue, a single ITCZ pattern in the tropical eastern Pacific, and the ENSO phase-locking to the annual cycle. However, simulated strengths of SST variability in the eastern equatorial Pacific and the phase locking to the annual cycle are larger than observed, and the westward propagation of zonal wind stress in the equatorial Pacific cannot be reproduced by the model. Atmospheric responses to ENSO are also simulated realistically by ECHO-G. The model belongs to the Group I category defined by AchutaRao and Sperber (2002) which comprises the CCMs with best skill in reproducing atmospheric responses to ENSO: the positive phase of ENSO, i.e. El Niño, is associated with a well-structured weakening of the Walker circulation, an enhanced warming extending from the tropical central Pacific to the west coast of South America, an associated rainfall in the tropical Pacific, and a warming over northern North America.

The observed variability of NH wintertime MSLP is characterized by two centers of action over the North Atlantic and the North Pacific. The pattern of MSLP variability in ECHO-G CTL shows locations and amplitudes similar to the observed. A near white noise spectrum of the detrended NAO index is obtained for the observations and the model simulation. The observed atmospheric patterns associated with the NAO are compared with the simulated patterns. The quadruple T2m structure over the Atlantic sector, wet and dry conditions over northern and southern Europe respectively, and the dominant dipole structure of MSLP over the Atlantic are well reproduced by ECHO-G CTL. While the observed MSLP has little correlation with the NAO index over the Pacific sector, the modeled MSLP reveals significant positive correlations over the North Pacific. This is a common problem found in many AOGCMs which might be caused by a too strong Atlantic-Pacific teleconnection. In summary, it can be said that ECHO-G performs well relative to the other coupled models it was compared with, despite its relatively coarse resolution.

A simple detection study of global mean T2m shows that the recent global positive 20-146 year trends cannot be explained by the internal variability of ECHO-CTL consistent with previous studies with other models (e.g. Collins et al. 2001 for HadCM3). Also, a simple trend analysis shows that the observed positive trend of the NAO index in the recent 40-60 years cannot be found in the 1000-year run, while the recent 10-30 year trends are simulated with a chance of more than 1%. This is in accordance with previous work using HadCM2 and HadCM3 control runs (Osborn et al. 1999; Collins et al. 2001). However, the

detection of anthropogenic effect on NAO is still controversial because of model-dependent responses of the NAO to greenhouse-gas warming and the signal-contaminated observations (e.g. SST).

Acknowledgements

This analyses was performed in the project “Research on the Development of Regional Climatic Change Scenarios to Prepare the National Climate Change Report (II)” of the Korean Meteorological Research Institute. The model was run on a NEC SX-4 at the DKRZ, Hamburg, Germany.

References

AchutaRao K, Sperber KR (2002) Simulation of the El Niño Southern Oscillation: Results from the Coupled Model Intercomparison Project. Clim Dyn **19**:191-209

Baquero-Bernal A, Latif M, Legutke S (2002) On dipolelike variability of sea surface temperature in the tropical Indian Ocean. J Clim **15**: 1358-1368

Barnett TP, Hasselmann K, Chelliah M, Delworth T, Hegerl G, Jones P, Ramusson E, Roeckner E, Ropelewski C, Santer B, Tett S (1999) Detection and attribution of recent climate change: A status report. Bull Amer Meteor Soc **80**: 2631-2659

Blanke B, Neelin JD, Gutzler D (1997) Estimating the effect of stochastic wind stress forcing on ENSO irregularity. J Clim **10**: 1473-1486

Braganza K, Karoly DJ, Hirst AC, Mann ME, Stott P, Stouffer RJ, Tett SFB (2002) Simple indices of global climate variability and change: Part I - variability and correlation structure. Clim Dyn **20**: 491-502

Bretherton CS, Battisti DS (2000) An interpretation of the results from atmospheric general circulation models forced by the time history of the observed sea surface temperature distribution. Geophys Res Lett **27**: 767-770

Chang P, Wang B, Li T, Ji L (1994) Interactions between the seasonal cycle and the southern oscillation – frequency entrainment and chaos in a coupled ocean-atmosphere model. Geophys Res Lett **21**: 817-820

Collins M (2000) The El-Niño-Southern Oscillation in the second Hadley Centre coupled model and its response to greenhouse warming. J Clim **13**: 1299-1312

Collins M, Tett SFB, Cooper C (2001) The internal climate variability of HadCM3, a version of the Hadley Centre coupled model without flux adjustments. Clim Dyn **17**: 61-81

Davey MK, Huddleston M, Sperber KR, Braconnot P, Bryan F, Chen D, Colman RA, Cooper C, Cubasch U, Delecluse P, DeWitt D, Fairhead L, Flato G, Gordon C, Hogan T, Ji M, Kimoto M, Kitoh A, Knutson TR, Latif M, Le Treut H, Li T, Manabe S, Mechoso CR, Meehl GA, Power SB, Roeckner E, Terray L, Vintzileos A, Voss R, Wang B, Washington WM, Yoshikawa I, Yu J-Y, Yukimoto S, Zebiak SE (2002) STOIC: A study of coupled model climatology and variability in tropical ocean regions. Clim Dyn **18**: 403-420

Eckert C, Latif M (1997) Predictability of a stochastically forced hybrid coupled model of El Niño. J Clim **10**: 1488-1504

Fedorov A, Philander SG (2000) Is El-Niño changing? Science **288**: 1997-2002

Frey H, Latif M, Stockdale T (1997) The coupled GCM ECHO-2. Part I: The tropical

Pacific. Mon Wea Rev **125**: 703-720

Fyfe JC, Boer GJ, Flato GM (1999) The Arctic and Antarctic Oscillations and their projected changes under global warming. Geophys Res Lett **26**: 1601-1604

Gillet NP, Allen MR, Tett SFB (2000) Modelled and observed variability in atmospheric vertical temperature structure. Clim Dyn **16**: 49-61

Glowienka-Hense R (1990) The North Atlantic Oscillation in the Atlantic-European SLP. Tellus **42**A: 497-507

Grötzner A, Latif M, Barnett TP (1998) A decadal climate cycle in the North Atlantic Ocean as simulated by the ECHO coupled GCM. J Clim **11**: 831-847

Grötzner A, Sausen R, Claussen M (1996) The impact of sub-grid scale sea-ice inhomogeneities on the performance of the atmospheric general circulation model ECHAM3, Clim Dyn **12**: 477-496

Guilyardi E, Delecluse P, Gualdi S, Navarra A (2003) Mechanisms for ENSO phase change in a coupled GCM. J Clim **16**: 1141-1158

Guilyardi E, Gualdi S, Slingo J, Navarra A, Delecluse P, Cole J, Madec G, Roberts M, Latif M, Terray L (2004) Representing El Niño in coupled ocean-atmosphere GCMs: the dominant role of the atmosphere component. J Clim (in press)

Hasselmann K (1976) Stochastic climate models, Part 1: Theory. Tellus **28**: 473-485

Hibler III WD (1979) A dynamic thermodynamic sea ice model. J Phys Oceanogr **9**: 817-846

Hirst AC, O'Farrell SP, Gordon HB (2000) Comparison of a coupled ocean–atmosphere model with and without oceanic eddy-induced advection. Part I: Ocean spinup and control integrations. J Clim **13**: 139-163

Hoerling MP, Hurrell JW, Xu T (2001) Tropical origins for recent North Atlantic climate change. Science **292**: 90-93

Hu ZZ, Latif M, Roeckner E, Bengtsson L (2000) Intensified Asian summer monsoon and its variability in a coupled model forced by increasing greenhouse gas concentrations. Geophys Res Lett **27**: 2681-2684

Hulme M (1992) A 1951-80 global land precipitation climatology for the evaluation of General Circulation Models. Clim Dyn **7**: 57-72

Hurrell JM (1995) Decadal trends in the North Atlantic Oscillation: regional temperatures and precipitation. Science **269**: 676-679

Hurrell JM (1996) Influence of variations in extratropical wintertime teleconnections on Northern Hemisphere temperature. Geophys Res Lett **23**: 665-668

Hurrell JW, van Loon H (1997) Decadal variations in climate associated with the North Atlantic Oscillation. Clim Change **36**: 301-326

Jones PD, Jonsson T, Wheeler D (1997) Extension to the North Atlantic Oscillation using

early instrumental pressure observations from Gibraltar and South-West Iceland. Int J Climatol **17**: 1433-1450

Jones PD, Moberg A (2003) Hemispheric and large-scale surface air temperature variations: An extensive revision and an update to 2001. J Clim **16**: 206-223

Jones PD, New M, Parker DE, Martin S, Rigor IG (1999) Surface air temperature and its changes over the past 150 years. Rev Geophys **37**: 173-199

Josey S, Kent E, Taylor P (1999) New insights into the ocean heat budget closure problem from analysis of the SOC air-sea flux climatology. J Clim **12**: 2856-2880

Kistler R, Kalnay E, Collins W, Saha S, White G, Woollen J, Chelliah M, Ebisuzaki W, Kanamitsu M, Kousky V, van den Dool H, Jenne R, Fiorino M (2001) The NCEP-NCAR 50-year reanalysis: monthly means CD-ROM and documentation. Bull Amer Meteor Soc **82**: 247-267

Lambert SJ, Boer GJ (2001) CMIP1 evaluation and intercomparison of coupled climate models. Clim Dyn **17**: 83-106

Latif M, Barnett TP (1996) Decadal climate variability over the North Pacific and North America: dynamics and predictability. J Clim **9**: 2407-2423

Latif M, Barnnet TP (1994) Causes of decadal climate variability over the North Pacific and North Atlantic. Science **266**: 634-637

Latif M, Sperber K, Arblaster J, Braconnot P, Chen D, Colman A, Cubasch U, Cooper C, Delecluse P, DeWitt D, Fairhead L, Flato G, Hogan T, Ji M, Kimoto M, Kitoh A, Knutson T, Le Treut H, Li T, Manabe S, Marti O, Mechoso C, Meehl G, Power S, Roeckner E, Sirven J, Terray L, Vintzileos A, Voss R, Wang B, Washington W, Yoshikawa I, Yu J, Zebiak S (2001) ENSIP: the El Niño simulation intercomparison project. Clim Dyn **18**: 255-276

Latif M, Stockdale T, Wolff J-O, Burgers G, Maier-Reimer E, Junge MM, Arpe K, Bengtsson L (1994) Climatology and variability in the ECHO coupled GCM. Tellus **46**A: 351-366

Legutke S (2000) Sea ice in coupled climate models: Impact of high-latitude freshwater fluxes. WCRP informal report No. 6: 25-28

Legutke S, Cubasch U (2000) A 1000-year control integration of the AOGCM ECHO-G. Research activities in atmospheric and oceanic modeling. CAS/JSC Working Group on Numerical Experimentation. Report No. 29

Legutke S, Maier-Reimer E (1999) Climatology of the HOPE-G global ocean general circulation model. Technical report No. 21, German Climate Computer Centre (DKRZ), Hamburg, Germany, 90 pp

Legutke S, Maier-Reimer E, Cubasch U, Hellbach A (1996) Sensitivity of an OGCM to the

resolution of atmospheric forcing data. CAS/JSC Working Group Numerical Experimentation, Report No. 26

Legutke S, Voss R (1999a) The Hamburg atmosphere-ocean coupled circulation model ECHO-G. Technical report No. 18, German Climate Computer Centre (DKRZ), Hamburg, Germany, 62 pp

Legutke S, Voss R (1999b) The ECHO-G coupled AOGCM. Research activities in atmospheric and oceanic modeling. CAS/JSC Working Group on Numerical Experimentation. Report No. 28, 9.8-9.9

Manabe S, Stouffer RJ (1996) Low-frequency variability of surface air temperature in a 1000-year integrations of a coupled atmosphere-ocean-land surface model. J Clim **9**: 376-393

Marshall GJ (2003) Trends in the Southern Annular Mode from observations and reanalyses. J Clim **16**: 4134–4143

Marshall GJ, Harangozo SA (2000) An appraisal of NCEP/NCAR reanalysis MSLP data viability for climate studies in the South Pacific. Geophys Res Lett **27**: 3957-3060

Marsland SJ, Latif M, Legutke S (2003) Antarctic circumpolar modes in a coupled ocean-atmosphere model. Ocean Dynamics **53**: 323-331

Mechoso CR, Robertson AW, Barth N, Davey MK, Delecluse P, Gent PR, Ineson S, Kirtman B, Latif M, Le Treut H, Nagai T, Neelin JD, Philander SGH, Polcher J, Schopf PS, Stockdale T, Suarez MJ, Terray L, Thual O, Tribbia JJ (1995) The seasonal cycle over the tropical Pacific in coupled ocean-atmosphere general circulation models. Mon Wea Rev **123**: 2825-2838

Osborn TJ, Briffa KR, Tett SFB, Jones PD, Trigo RM (1999) Evaluation of the North Atlantic Oscillation as simulated by a coupled climate model. Clim Dyn **15**: 685-702

Paeth H, Hense A, Glowienka-Hense R, Voss R, Cubasch U (1999) The North Atlantic Oscillation as an indicator for greenhouse-gas induced regional climate change. Clim Dyn **15**: 953-960

Paeth H, Latif M, Hense A (2003) Global SST influence on twentieth century NAO variability. Clim Dyn **21**: 63-75

Pierce DW, Barnett TP, Latif M (2000) Connections between the Pacific Ocean tropics and midlatitudes on decadal timescales. J Clim **13**: 1173-1194

Rayner NA, Horton EB, Parker DE, Folland CK, Hackett RB (1996) Version 2.2 of the global sea-ice and sea surface temperature data set, 1903-1994. Hadley Centre Climate Research Techn Note, CRTN 74, Sept., 1996, Hadley Centre, Meteorological Office, Bracknell, UK, 21 pp

Rayner NA, Parker DE, Horton EB, Folland CK, Alexander LV, Rowell DP, Kaplan A, Kent

EC, Kaplan A (2003) Global analyses of SST, sea ice and night marine air temperature since the late nineteenth century. J Geophys Res **108**(D14): 4407 DOI 10.1029/2002JD002670

Robertson AW, Mechoso CR, Kim YJ (2000) The influence of Atlantic sea surface temperature anomalies on the North Atlantic Oscillation. J Clim **13**:122-138

Rodgers KB, Friederichs P, Latif M (2004) Tropical Pacific decadal variability and its relation to decadal modulations of ENSO. J Clim (accepted)

Rodwell MJ, Rowell DP, Folland CK (1999) Oceanic forcing of the wintertime North Atlantic Oscillation and European climate. Nature **398**: 320-323

Roeckner E, Arpe K, Bengtsson L, Christoph M, Claussen M, Dümenil L, Esch M, Giorgetta M, Schlese U, Schulzweida U (1996a) The atmospheric general circulation model ECHAM-4: model description and simulation of present-day climate. Report No. 218, Max Planck Institute for Meteorology, Hamburg, Germany, 90 pp

Roeckner E, Bengtsson L, Feichter J, Lelieveld J, Rodhe H (1999) Transient climate change simulations with a coupled atmosphere–ocean GCM including the tropospheric sulfur cycle. J Clim **12**: 3004-3032

Roeckner E, Oberhuber JM, Bacher A, Christoph M, Kirchner I (1996b) ENSO variability and atmospheric response in a global coupled atmosphere-ocean GCM. Clim Dyn **12**: 737-754

Rogers JC (1984) The association between the North Atlantic Oscillation and the Southern Oscillation in the Northern Hemisphere. Mon Wea Rev **112**: 1999-2015

Rogers JC (1990) Patterns of low-frequency monthly sea level pressure variability (1899–1986) and associated wave cyclone frequencies. J Clim **3:** 1364–1379

Ropelewski CF, Halpert MS (1987) Global and regional scale precipitation patterns associated with the El Niño/Southern Oscillation. Mon Wea Rev **115**: 1606-1626

Schneider N, Barnett T, Latif M, Stockdale T (1996) Warm pool physics in a coupled GCM. J Clim **9**: 219-239

Shindell DT, Miller RL, Schmidt G, Pandolfo L (1999) Simulation of the Arctic Oscillation trend by greenhouse forcing of a stratospheric model. Nature **399**: 452-455

Stendel M, Erich Roeckner (1998) Impacts of horizontal resolution on simulated climate statistics in ECHAM4. Report No. 253, Max Planck Institute for Meteorology, 57 pp

Stephenson DB, Pavan V (2003) The North Atlantic Oscillation in coupled climate models: a CMIP1 evaluation. Clim Dyn **20**: 381-399

Stephenson DB, Pavan V, Bojariu R (2000) Is the North Atlantic Oscillation a random walk? Int J Climatol **20**: 1-18

Stouffer RJ, Hegerl G, Tett S (2000) A comparison of surface air temperature variability in

three 1000-yr coupled ocean-atmosphere model integrations. J Clim **13**: 513-537

Valcke S, Terray L, Piacentini A (2000) The OASIS Coupler User Guide, Version 2.4, Technical report TR/CMGC/00-10, CERFACS, 77 pp

Tett SFB, Johns TC, Mitchell JFB (1997) Global and regional variability in a coupled AOGCM. Clim Dyn **13**: 303-323

Thompson DWJ, Wallace JM (1998) The Arctic Oscillation signature in the wintertime geopotential height and temperature fields. Geophys Res Lett **25**: 1297-1300

Thompson DWJ, Wallace JM (2000) Annular modes in the extratropical circulation. Part I: Month-to-month variability. J Clim **13**: 1000–1016

Thompson DWJ, Wallace JM (2001) Regional climate impacts of the Northern Hemisphere Annular Mode. Science **293**: 85-89

Timmermann A, Latif A, Voss R, Grötzner A (1998) Northern Hemisphere interdecadal variability: a coupled air-sea mode. J Clim **11**: 1906-1931

Timmermann M, Latif A, Grötzner A, Voss R (1999) Modes of climate variability as simulated by a coupled general circulation model. Part I: ENSO-like variability and its low-frequency modulation. Clim Dyn **15**: 605-618

Trenberth KE, Caron JM (2000) The Southern Oscillation revisited: sea level pressures, surface temperatures, and precipitation, J Clim **13**: 4358-4365

van Loon H, Madden RA (1981) The Southern Oscillation. Part I: global associations with pressure and temperature in northern winter. Mon Wea Rev **109**: 1150-1162

Venzke S, Latif M, Villwock A (2000) The coupled GCM ECHO-2. Part II: Indian Ocean response to ENSO. J Clim **13**: 1371-1383

Vimont DJ, Battisti DS, Hirst AC (2002) Pacific interannual and interdecadal equatorial variability in a 1000-yr simulation of the CSIRO coupled general circulation model. J Clim **15**: 160-178

von Storch JS, Kharin VV, Cubasch U, Hegerl GC, Schriever D, von Storch H, Zorita E (1997) A description of a 1260-year control integration with the coupled ECHAM1/LSG general circulation model. J Clim **10**: 1525-1543

von Storch JS, Müller P, Bauer E (2001) Climate variability in millennium integrations with coupled atmosphere-ocean GCMs: a spectral view. Clim Dyn **17**: 375-389

von Storch JS, Müller P, Stouffer RJ, Voss R, Tett SFB (2000) Variability of deep-ocean mass transport: spectral shapes and spatial scales. J Clim **13**: 1916-1935

Voss R, Sausen R, Cubasch U (1998) Periodically synchronously coupled integrations with the atmosphere-ocean general circulation model ECHAM3/LSG. Clim Dyn **14**: 249-266

Wolff J-O, Maier-Reimer E, Legutke S (1997) The Hamburg Ocean Primitive Equation

Model. Technical report No. 13, German Climate Computer Center (DKRZ), Hamburg, Germany, 98 pp

Wunsch C (1999) The Interpretation of Short Climate Records, with Comments on the North Atlantic and Southern Oscillations. Bull Amer Meteor Soc **80**(2): 245–256

Xie P, Arkin PA (1997) Global precipitation: A 17-year monthly analysis based on gauge observations, satellite estimates, and numerical model outputs. Bull Amer Meteor Soc **78**: 2539-2558

Zorita E, González-Rouco F, Legutke S (2003) Testing the Mann et al. (1998) approach to paleoclimate reconstructions in the context of a 1000-yr control simulation with the ECHO-G coupled climate model. J Clim **16**: 1378-1390

Table 1. List of millennium control integrations of AOGCMs and analyzed variables for the internal climate variability.

Model (Institution)	Total integration length (years)	Analyzed variables[a]	Resolutions (Atmosphere / Ocean)[b]	Flux corrections[c]	References
GFDL_R15_a (GFDL)	1000	T2m[1], SST, THC[2,3]	R15 (4.5×7.5) L9 / 4.5×3.7 L12	H, W	Manabe and Stouffer (1996)
ECHAM1/LSG (DKRZ)	1260	T2m, THC[2,3], V200[3], V500[3], V850[3],	T21 (5.6×5.6) L19 / 4.0×4.0 L11	M, H, W	von Storch et al. (1997)
ECHAM3/LSG (DKRZ)	1000	T2m[1], SST[3], THC[2,3]	T21 (5.6×5.6) L19 / 4.0×4.0 L11	M, H, W	Voss et al. (1998) Timmermann et al. (1999)
HadCM2 (UKMO)	1700	T2m[1,4], ZMT, THC[2,3], ENSO, NAO	2.5×3.75 L19 / 2.5×3.75 L20	H, W	Tett et al. (1997) Osborn et al. (1999) Gillett et al. (2000) Collins (2000)
HadCM3 (UKMO)	1000	T2m[4], ZMT, ENSO, NAO	2.5×3.75 L19 / 1.25×1.25 L20	-	Collins et al. (2001)
CSIRO Mk2 (CSIRO)	1000	T2m[4], ENSO	R21 (3.2×5.6) L9 / 3.2×5.6 L21	M, H, W	Hirst et al. (2000) Vimont et al. (2002)
ECHO-G (MPIfM, M&D)	1000	T2m, THC	T30 (3.75×3.75) L19 / 2.8×2.8[#] L20	H*, W*	Legutke and Cubasch (2000)

a. T2m (near surface temperature), ZMT (zonal mean temperature), SST (sea surface temperature), THC (thermohaline circulation), and V'mmm' ('mmm' hPa wind). The number 1, 2, 3, and 4 indicate the analysis done by Stouffer et al. (2000), von Storch et al. (2000), von Storch et al. (2001), and Braganza et al. (2002), respectively.

b. Latitude × longitude with a spectral truncation. A sharp (#) depicts the equatorial refinement (0.5 between 10°S-10°N). Vertical resolution is expressed as 'L' + number of vertical levels.

c. M (momentum flux), H (heat flux), and W (freshwater flux). An asterisk (*) indicates annual mean flux adjustment only.

Table 2. Observational data for each analyzed variable.

Variable (Abbreviation, Unit)	Source	Resolution	Analysis period	References
Near surface temperature (T2m, °C)	HadCRUT2	5°×5°	1856-2001	Jones and Moberg (2003) Rayner et al. (2003)
Sea surface temperature (SST, °C)	GISST2.2	1°×1°	1903-1994	Rayner et al. (1996)
Precipitation (PCP, mm/day)	CMAP	2.5°×2.5°	1979-1999	Xie and Arkin (1997)
	CRU-PCP	5°×5°	1900-1998	Hulme (1992)
Mean sea level pressure (MSLP, hPa)	NCEP/NCAR reanalysis	2.5°×2.5°	1958-2001	Kistler et al. (2001)
Zonal wind stress (none, N/m^2)	SOC	1°×1°	Climate (1980-1993)	Josey et al. (1999)
NAO index for DJFM (none, hPa)	CRU	-	1823/24-1999/2000	Jones et al. (1997)
NINO3 index (none, °C)	GISST2.2	-	1903-1994	-

Table 3. Trends of global temperature anomaly in the HadCRUT observation and corresponding trend occurrences greater than the observed trends in the ECHO-G CTL. Values in parenthesis denote the results from 'masked' ECHO-G CTL.

Observation period (years)	Trend length (years)	Observed trend (°C/century)	Model trend occurrence			
			Occurrence		Relative occurrence (%)	
1992-2001	10	3.2	23	(18)	2.3	(1.8)
1987-2001	15	1.6	73	(46)	7.4	(4.7)
1982-2001	20	2.0	0	(0)	0.0	(0.0)
1977-2001	25	1.8	0	(0)	0.0	(0.0)
1972-2001	30	1.9	0	(0)	0.0	(0.0)
1962-2001	40	1.4	0	(0)	0.0	(0.0)
1952-2001	50	1.0	0	(0)	0.0	(0.0)
1902-2001	100	0.7	0	(0)	0.0	(0.0)
1856-2001	146	0.5	0	(0)	0.0	(0.0)

Table 4. Trends of the observed NAO index and corresponding trend occurrences greater than the observed trends in the ECHO-G CTL.

Observation period (years)	Trend length (years)	Observed trend (hPa/year)	Model trend occurrence	
			Occurrence	Relative occurrence (%)
1990-99	10	-0.18	623	62.9
1980-99	20	0.12	279	28.5
1970-99	30	0.18	66	6.8
1960-99	40	0.25	0	0
1950-99	50	0.18	0	0
1940-99	60	0.11	3	0.3
1930-99	70	0.08	10	1.1
1920-99	80	0.02	184	20.0
1910-99	90	0.002	483	53.1
1900-99	100	-0.01	749	83.2
1823-99	177	0.001	395	48.0

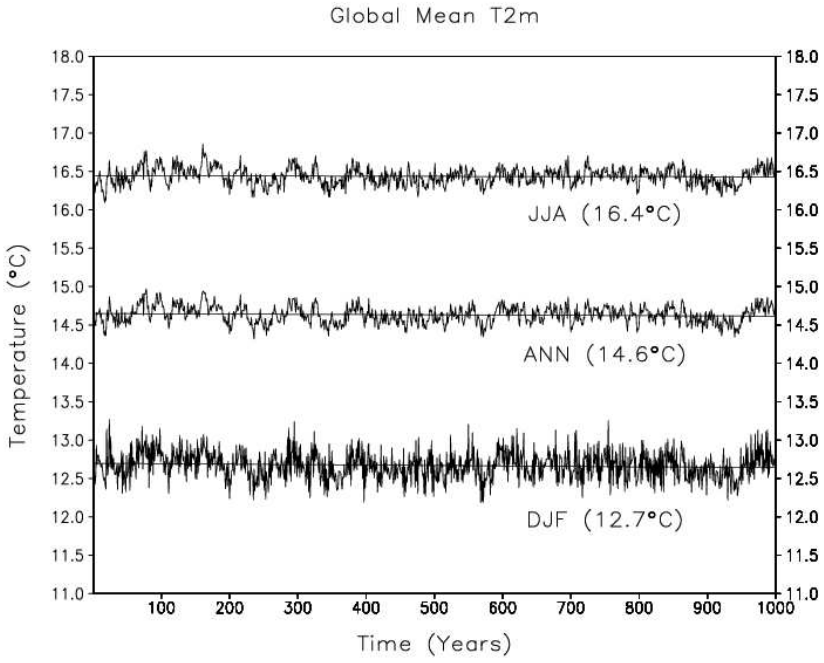

Figure 1 Annual (ANN) and seasonal (DJF, JJA) mean time series of global mean near surface temperature from ECHO-G CTL. Values in parentheses are 1000-year mean, and solid lines are linear trends. Observational values estimated from HadCRUT (1961-1990, Jones et al. 1999) are 14.1, 12.4, and 15.9°C for ANN, DJF, and JJA, respectively.

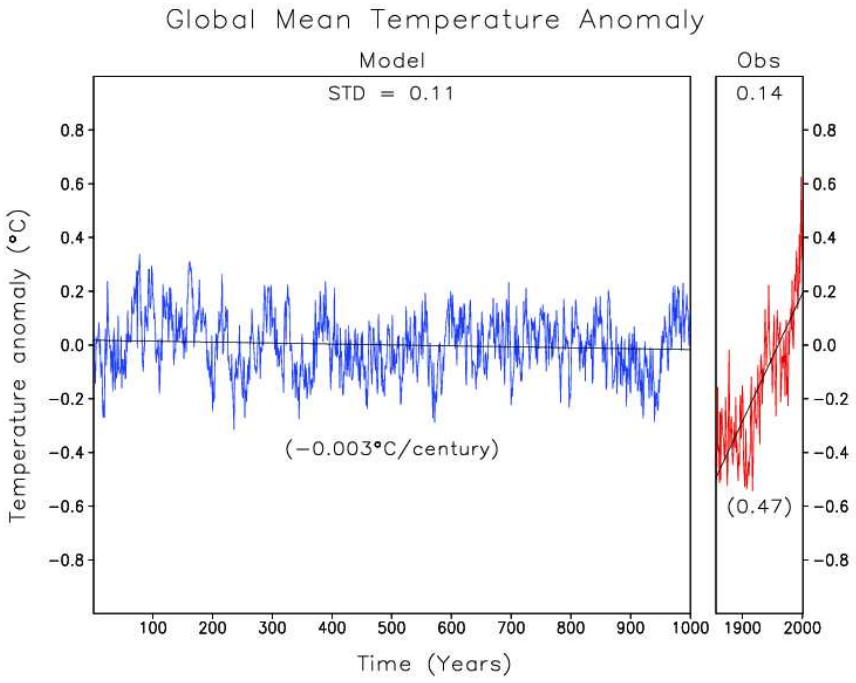

Figure 2 Time series of global (85°S-85°N) annual mean near surface temperature anomalies from ECHO-G CTL and HadCRUT observations (1856-2001). Solid lines are linear trends. Their values are given in parentheses (°C/century).

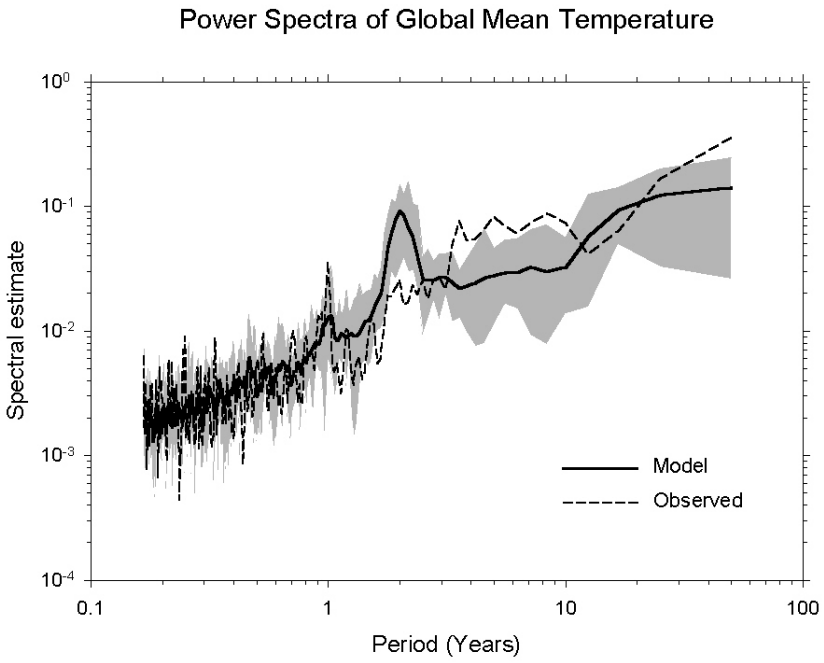

Figure 3 Power spectra of the global mean T2m from ECHO-G CTL (solid line) and HadCRUT observations (dashed line, 1901-2000). The shading indicates the maximum and minimum spectral estimates from ten 100-year sections of ECHO-G CTL and the solid line is an average of the ten power spectra.

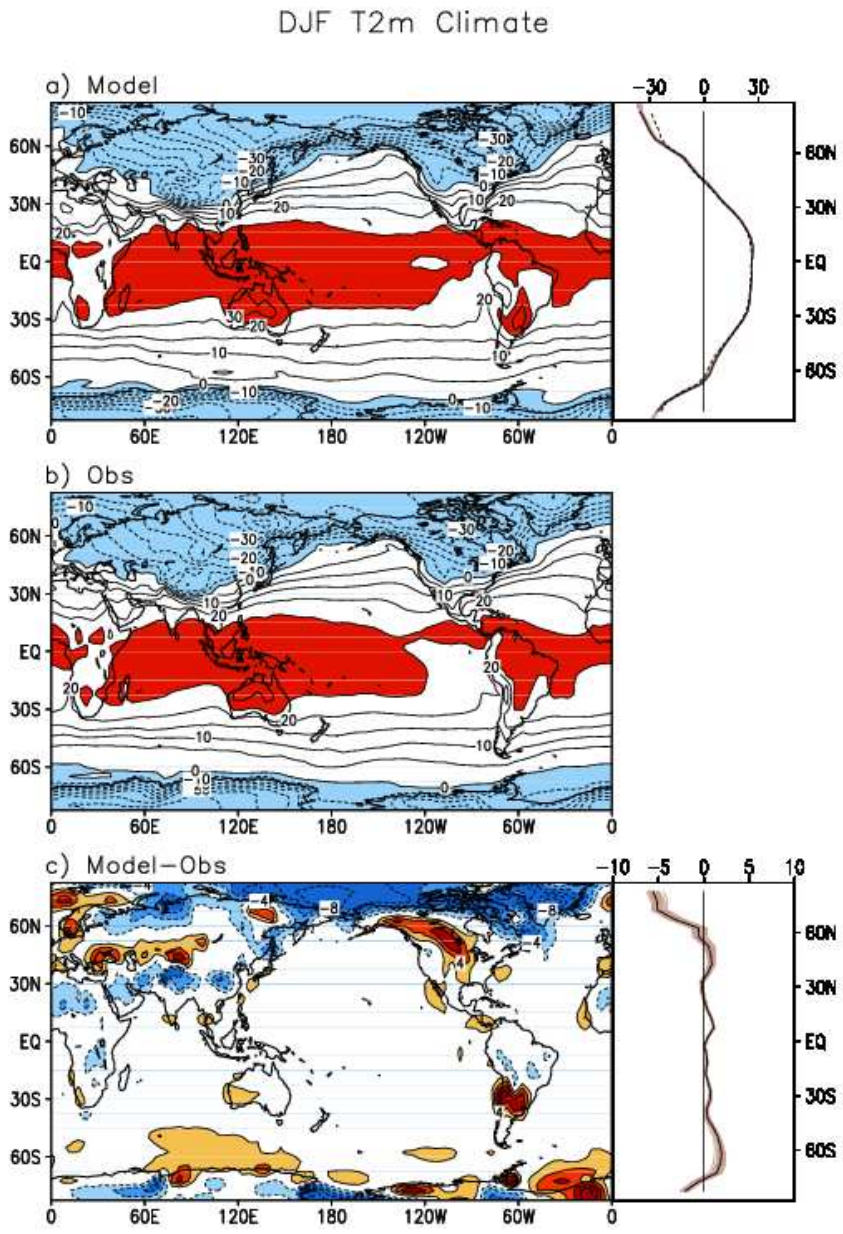

Figure 4 T2m climate in DJF for a) model, b) observations, c) model minus observation. Contour intervals are 5°C in a) and b) and 2°C in c). The zero line is omitted in c). Zonal means for the model (solid line) and the observation (dashed line) are plotted together in the upper right panel. The zonal mean of model biases is presented in the lower right panel. Light solid lines in the zonal mean plots represent the results from 33 30-year subsections of ECHO-G CTL.

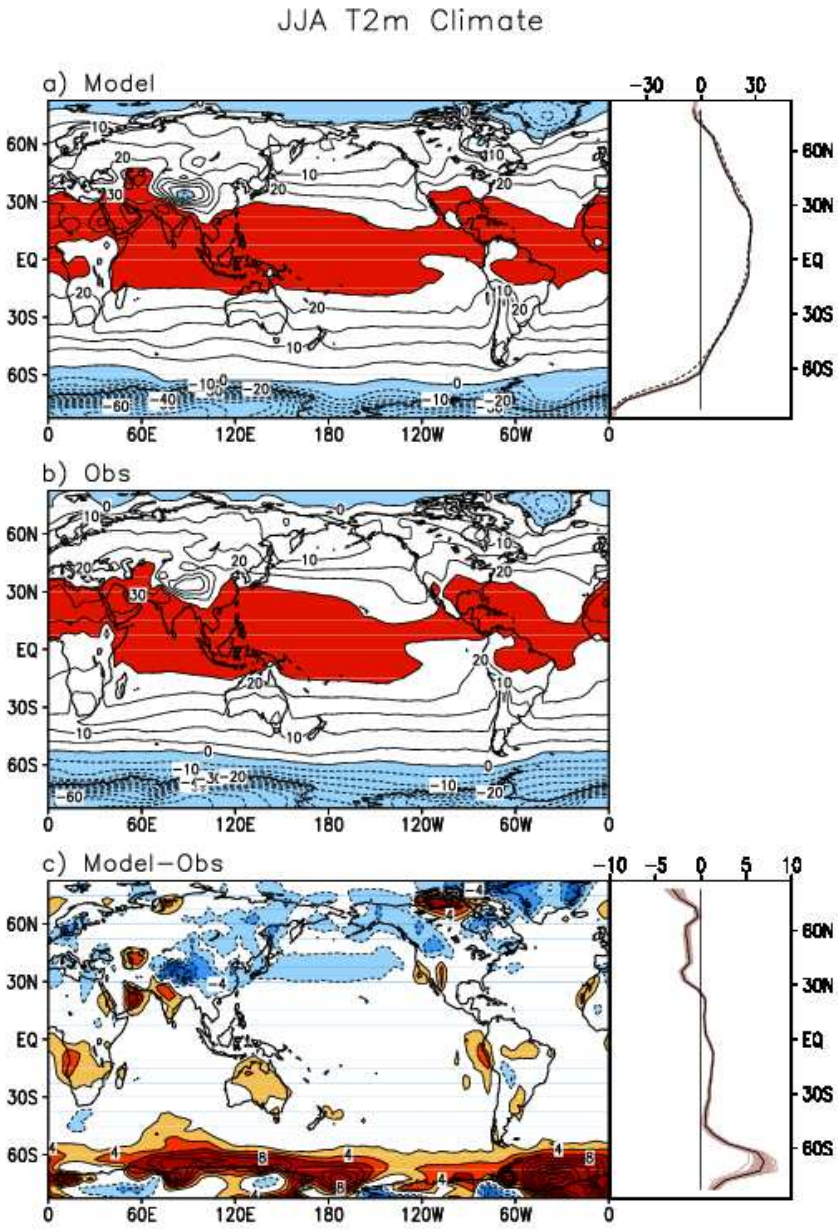

Figure 5 Same as Figure 4 but for JJA T2m.

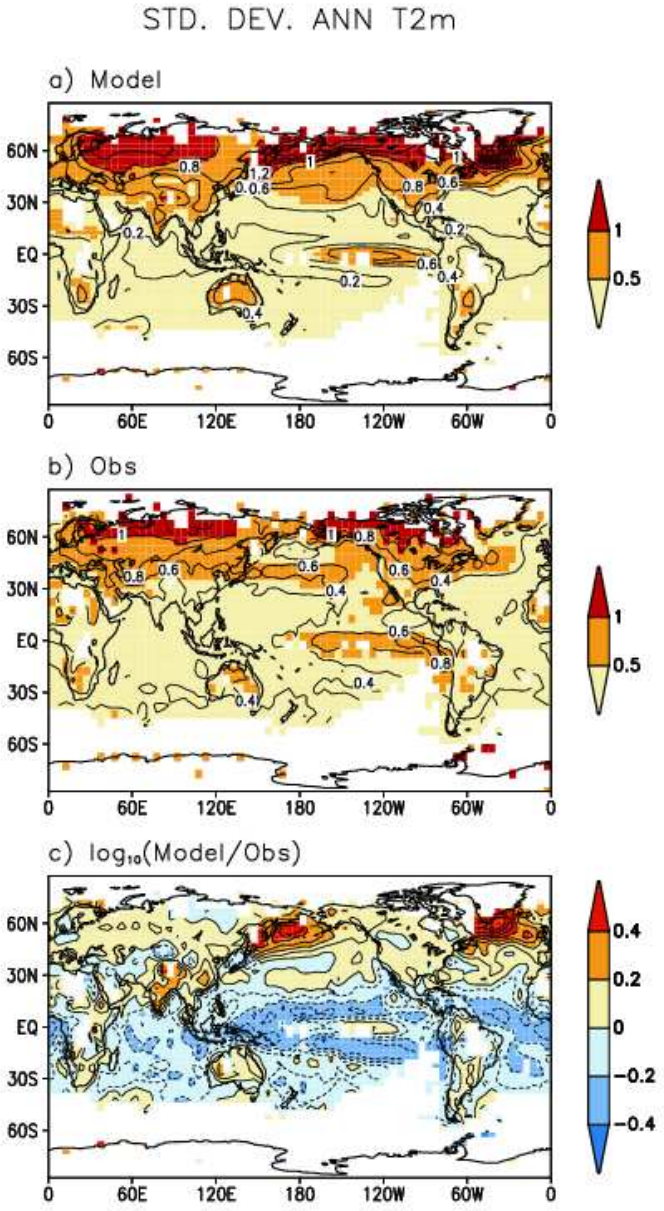

Figure 6 Spatial distribution of the standard deviation of annual mean surface temperature from a) ECHO-G CTL and b) HadCRUT observations and c) the logarithm of their ratio.

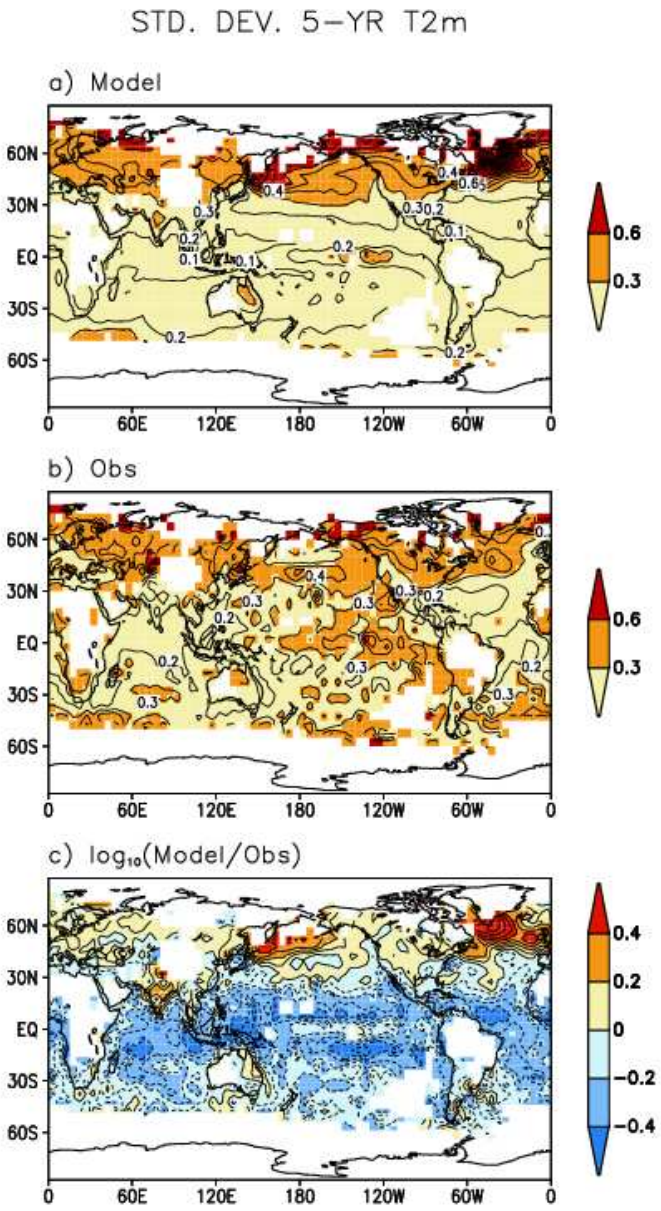

Figure 7 Same as Figure 6 but for 5-year mean T2m. Contour intervals are 0.1 for all panels.

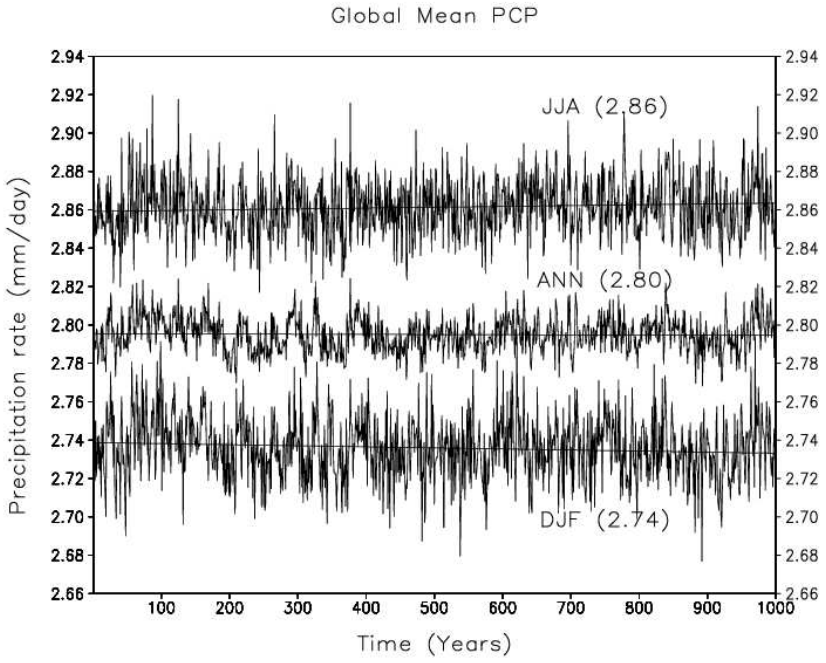

Figure 8 Same as Figure 1 but for PCP (mm/day). Observational values estimated from CMAP (1979-1998) are 2.68, 2.64, and 2.78 mm/day for ANN, DJF, and JJA, respectively.

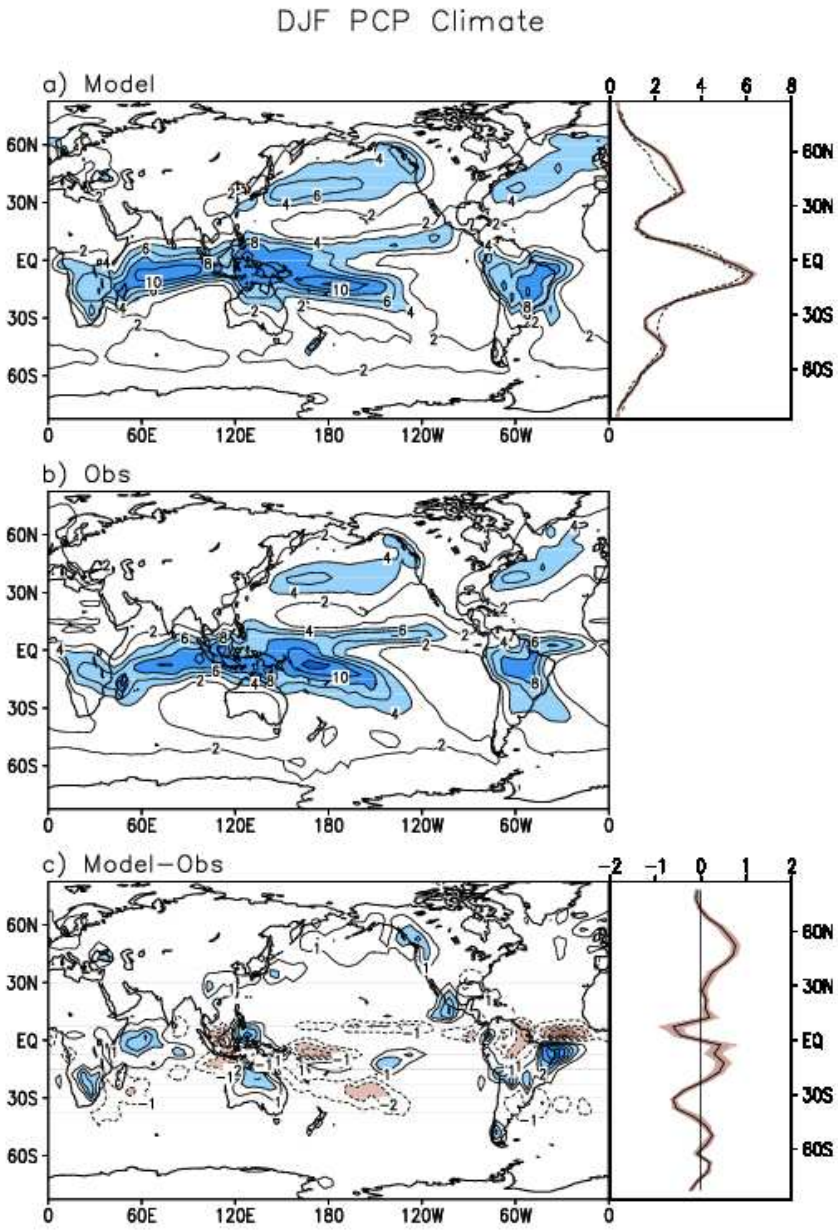

Figure 9 Same as Figure 4 but for DJF PCP (mm/day). Contour intervals are 2 in a) and b) and 1 in c). The zero line is omitted in c). Light solid lines in the zonal mean plots represent the results from 49 20-year subsections of ECHO-G CTL.

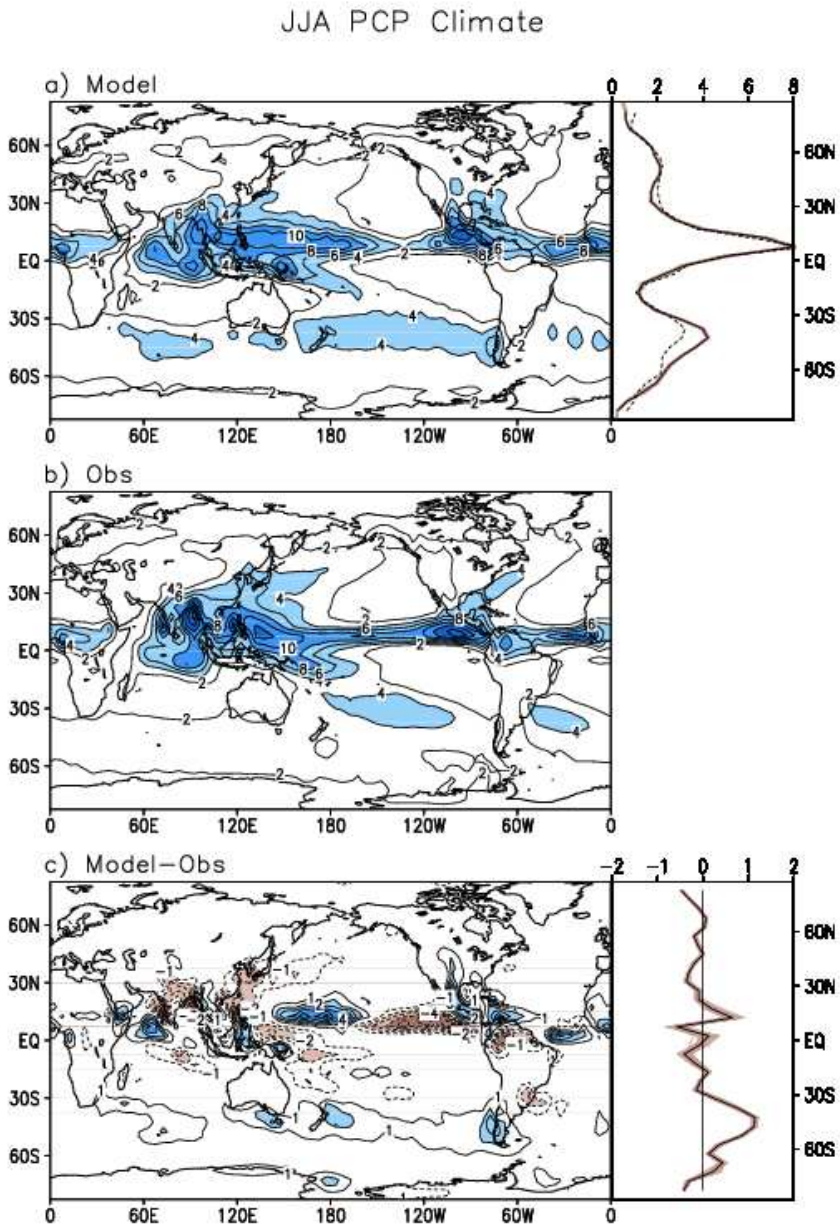

Figure 10 Same as Figure 4 but for JJA PCP (mm/day). Contour intervals are 2 in a) and b) and 1 in c). The zero line is omitted in c). Light solid lines in the zonal mean plots represent the results from 50 20-year subsections of ECHO-G CTL.

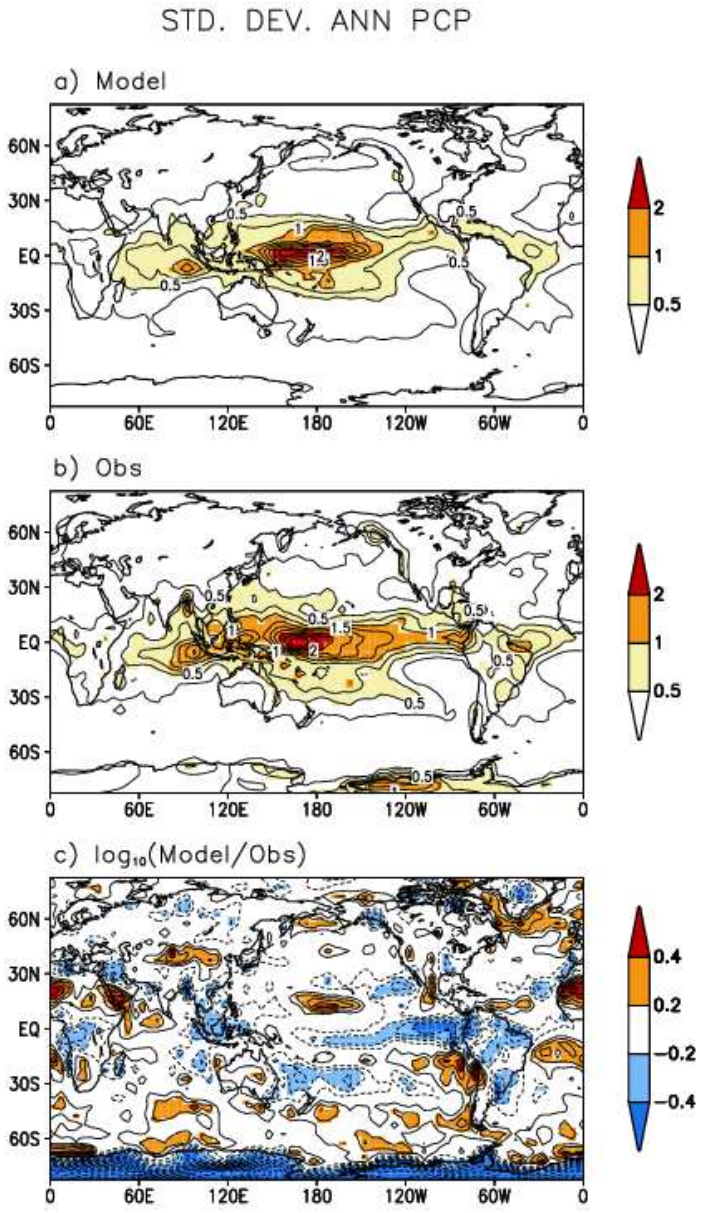

Figure 11 Same as Figure 6 but for precipitation (mm/day). Contour intervals are 0.5 in a) and b) and 0.1 in c). Solid lines are for positive values, dotted lines for negative values, and the zero line is omitted in c).

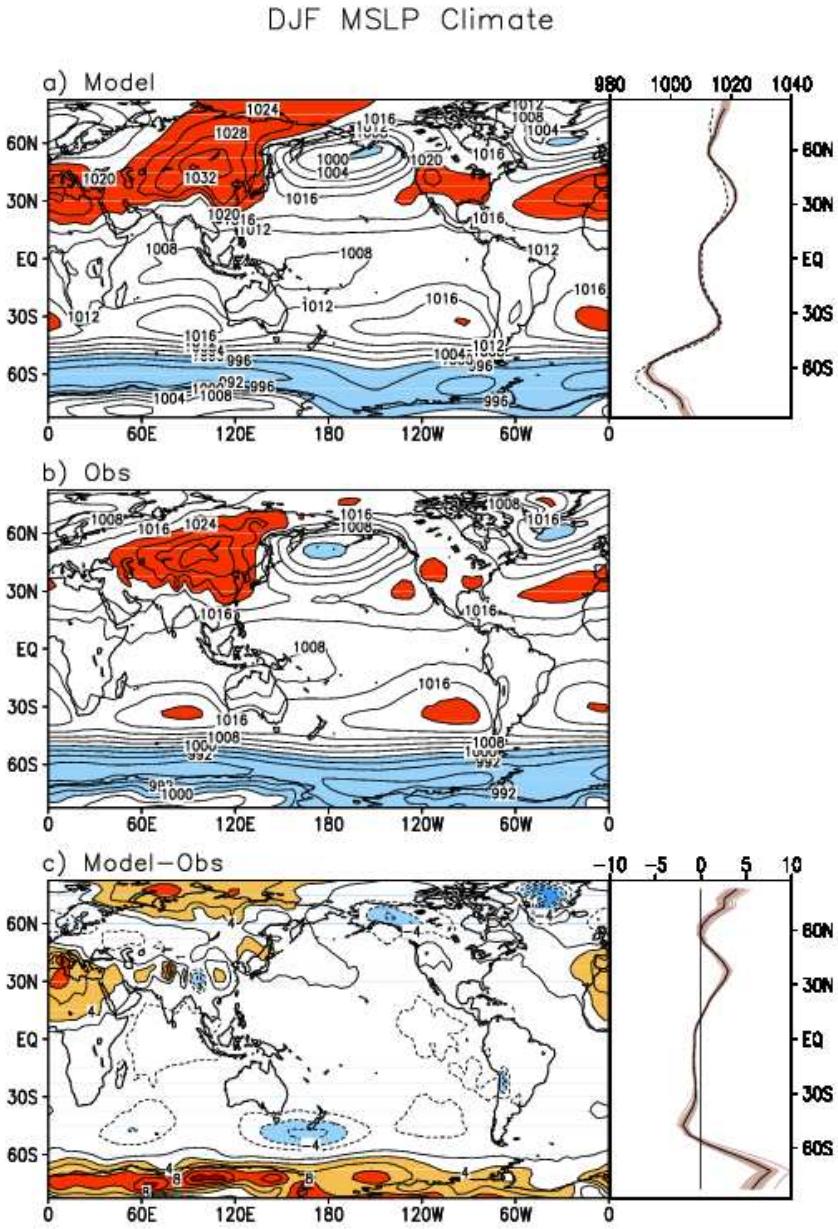

Figure 12 Same as Figure 4 but for DFJ MSLP (hPa). Light solid lines in the zonal mean plots represent the results from 33 30-year subsections of ECHO-G CTL.

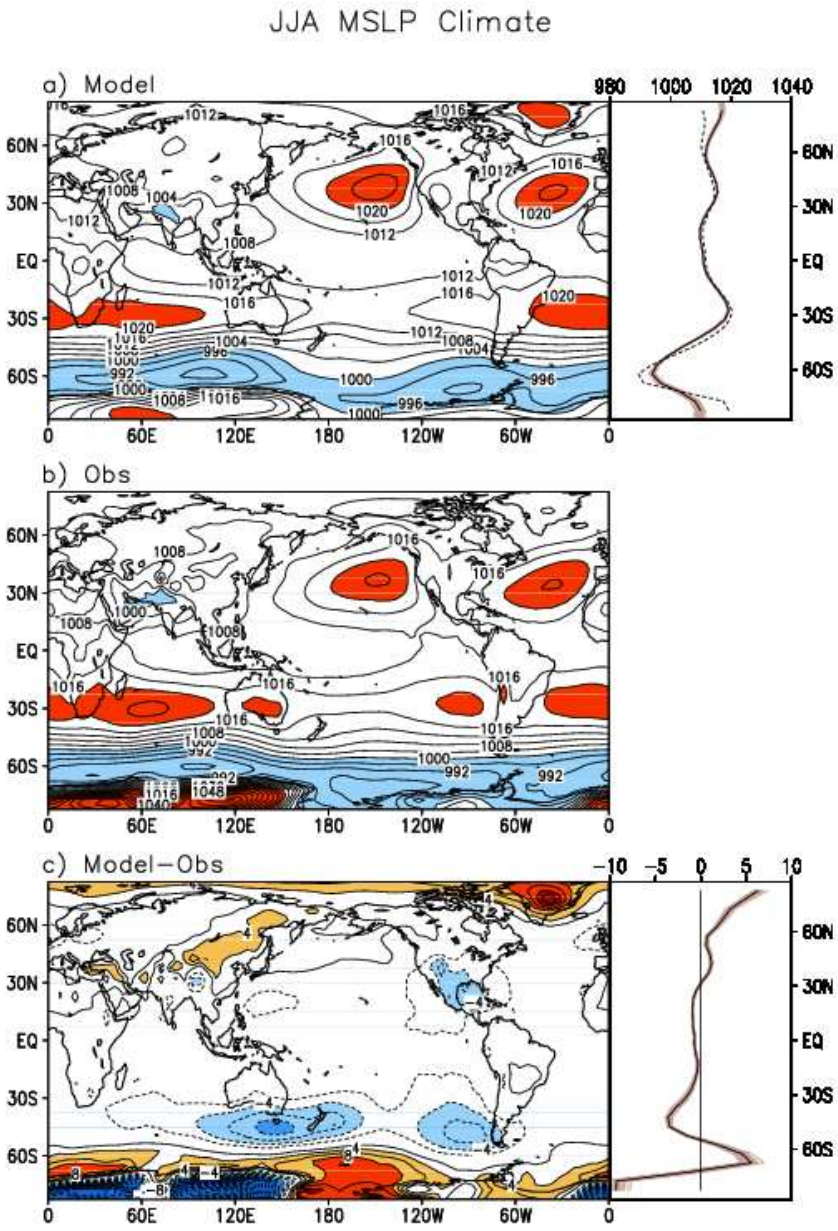

Figure 13 Same as Figure 5 but for JJA MSLP (hPa). Contour intervals are 4 hPa in a) and b) and 2 hPa in c). Solid lines are for positive values, dotted lines for negative values, and the zero line is omitted in c). Light solid lines in the zonal mean plots represent the results from 33 30-year subsections of ECHO-G CTL.

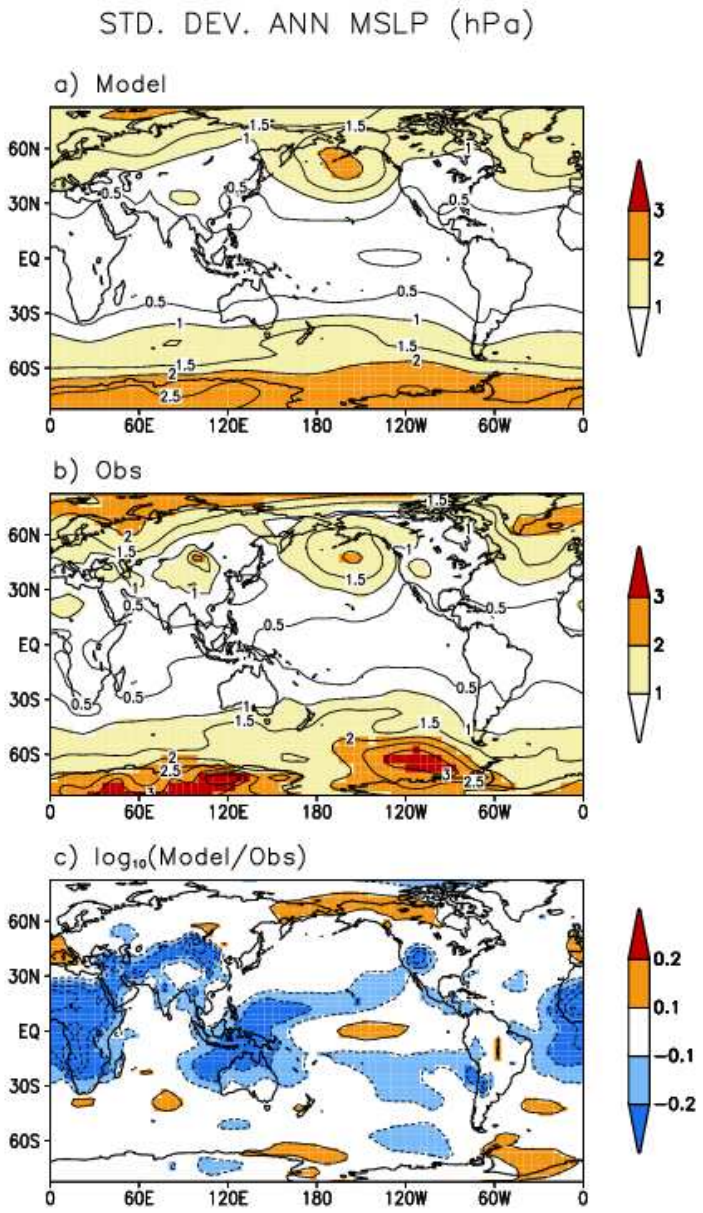

Figure 14 Same as Figure 6 but for MSLP (hPa). Contour intervals are 0.5 hPa in a) and b) and 0.1 in c). Solid lines are for positive values, dotted lines for negative values, and the zero line is omitted in c).

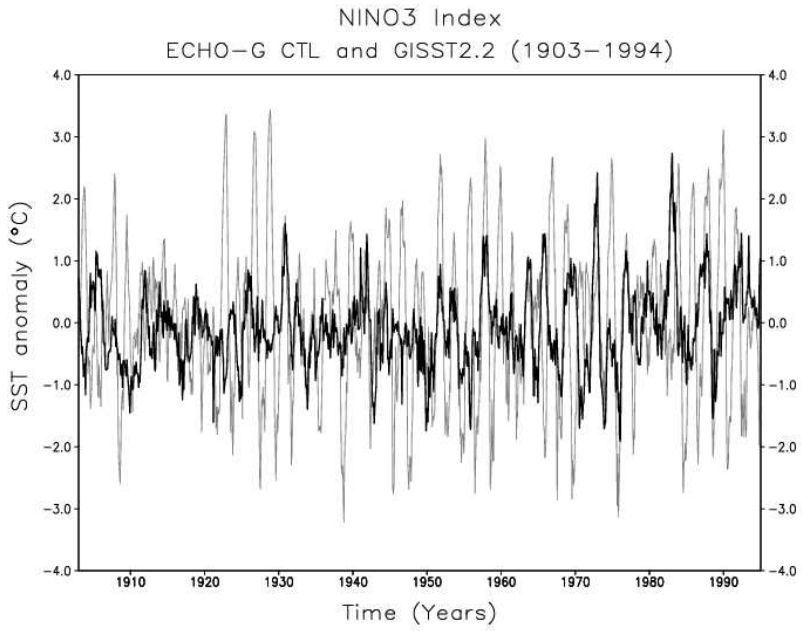

Figure 15 Time series of the monthly NINO3 index from ECHO-G CTL (thin line) and GISST2.2 (thick line) from 1903 to 1994. The first 92 years of the 1000-year ECHO-G CTL are plotted.

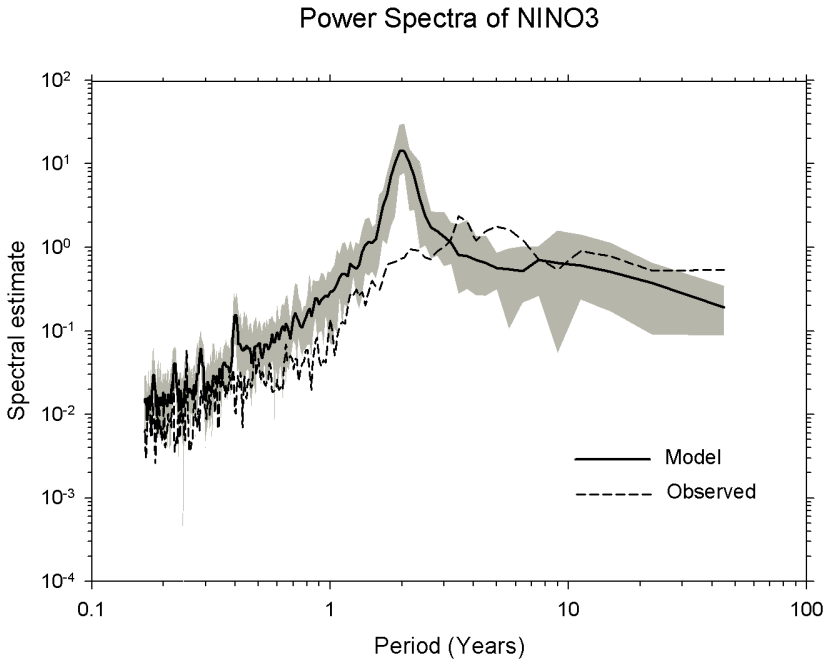

Figure 16 Power spectra of the NINO3 index from ECHO-G CTL (solid line) and the observed NINO3 index (GISST, 1905-1994). The shading indicates the maximum and minimum spectra from 11 90-year sections of ECHO-G CTL and the solid line is the average of the 11 spectra.

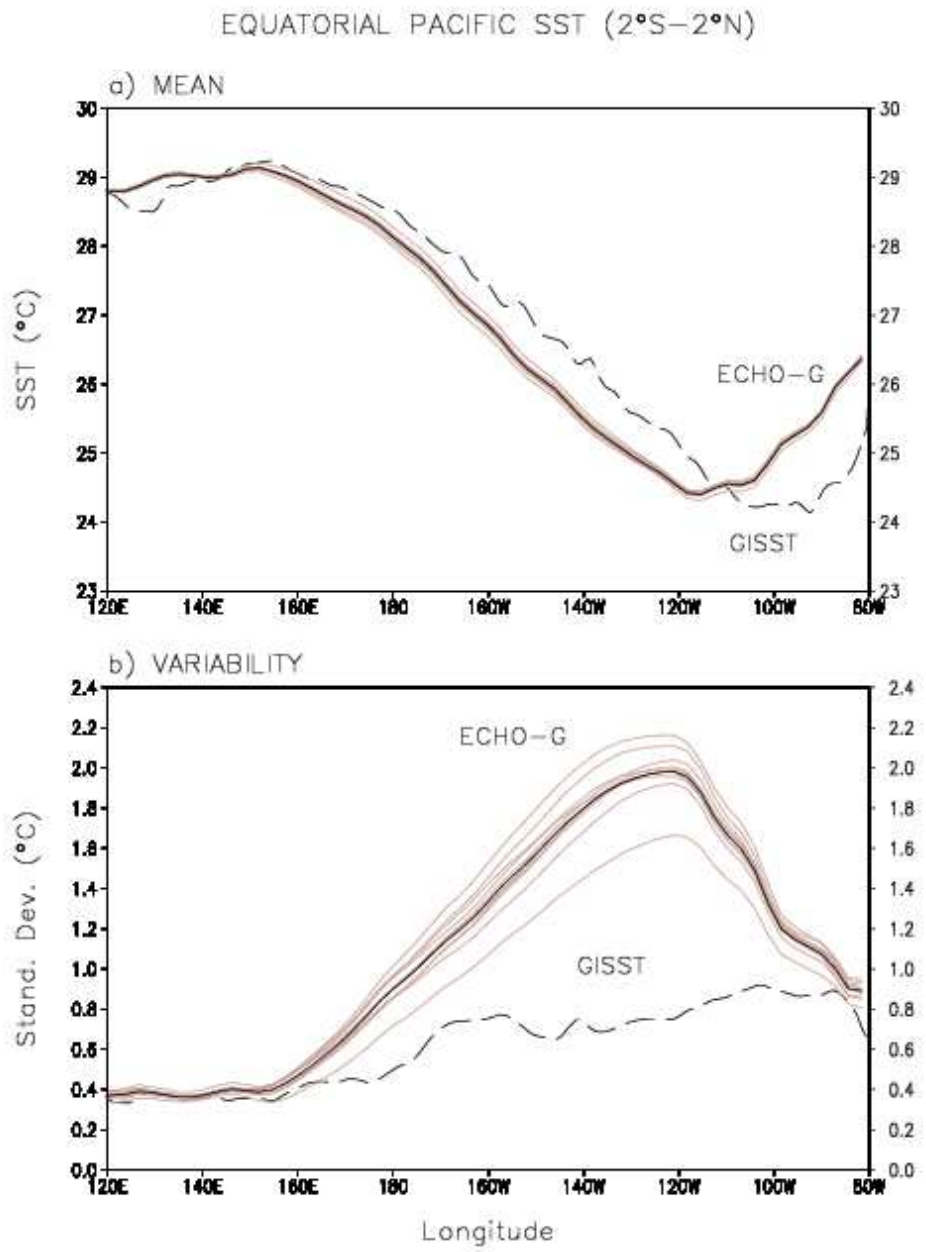

Figure 17 a) Climatological mean SST and b) standard deviation of SST anomalies from monthly mean climatology in the equatorial Pacific (2°S-2°N) for ECHO-G CTL and GISST (1903-1994). Light solid lines represent the results from ten 92-year subsections of ECHO-G CTL.

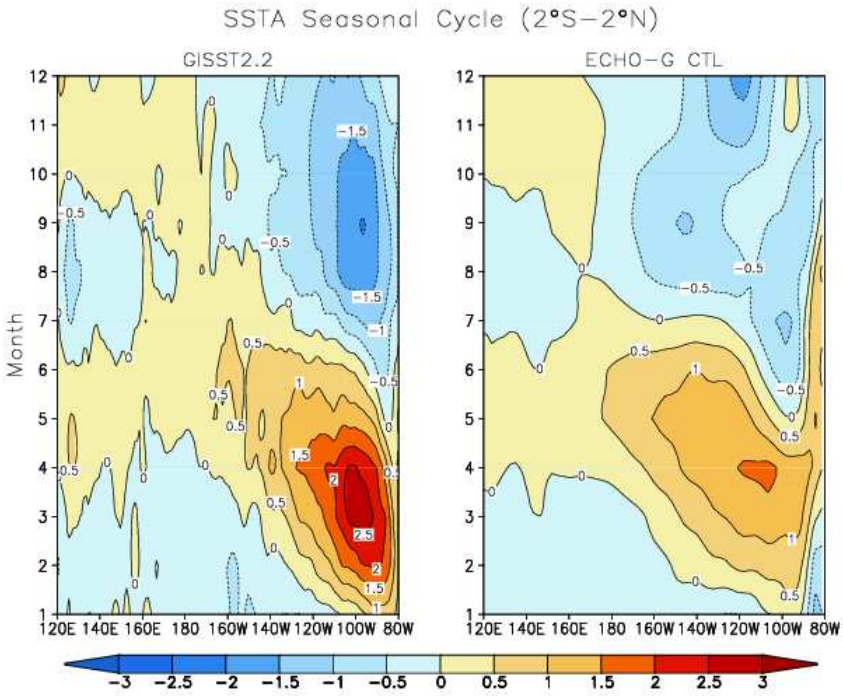

Figure 18 Annual cycle of equatorial (2°S-2°N) Pacific SST anomalies (°C) for ECHO-G CTL (right) and GISST (1903-1994, left).

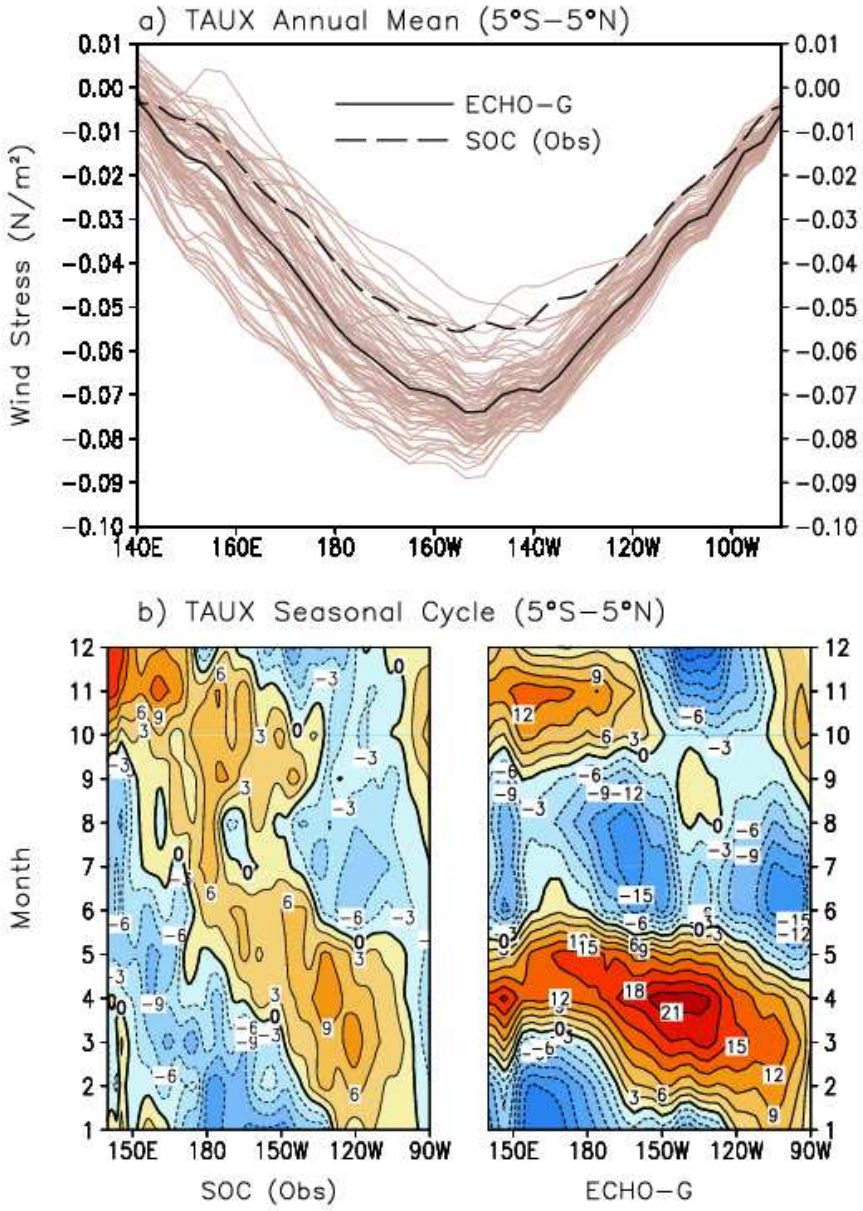

Figure 19 a) Longitudinal annual mean and b) annual cycle distribution of zonal wind stress (N/m^2) in the equatorial (5°S-5°N) Pacific for the SOC observation (1980-1993, left) and ECHO-G CTL (right). Light solid lines in a) represent the results from 71 14-year subsections of ECHO-G CTL.

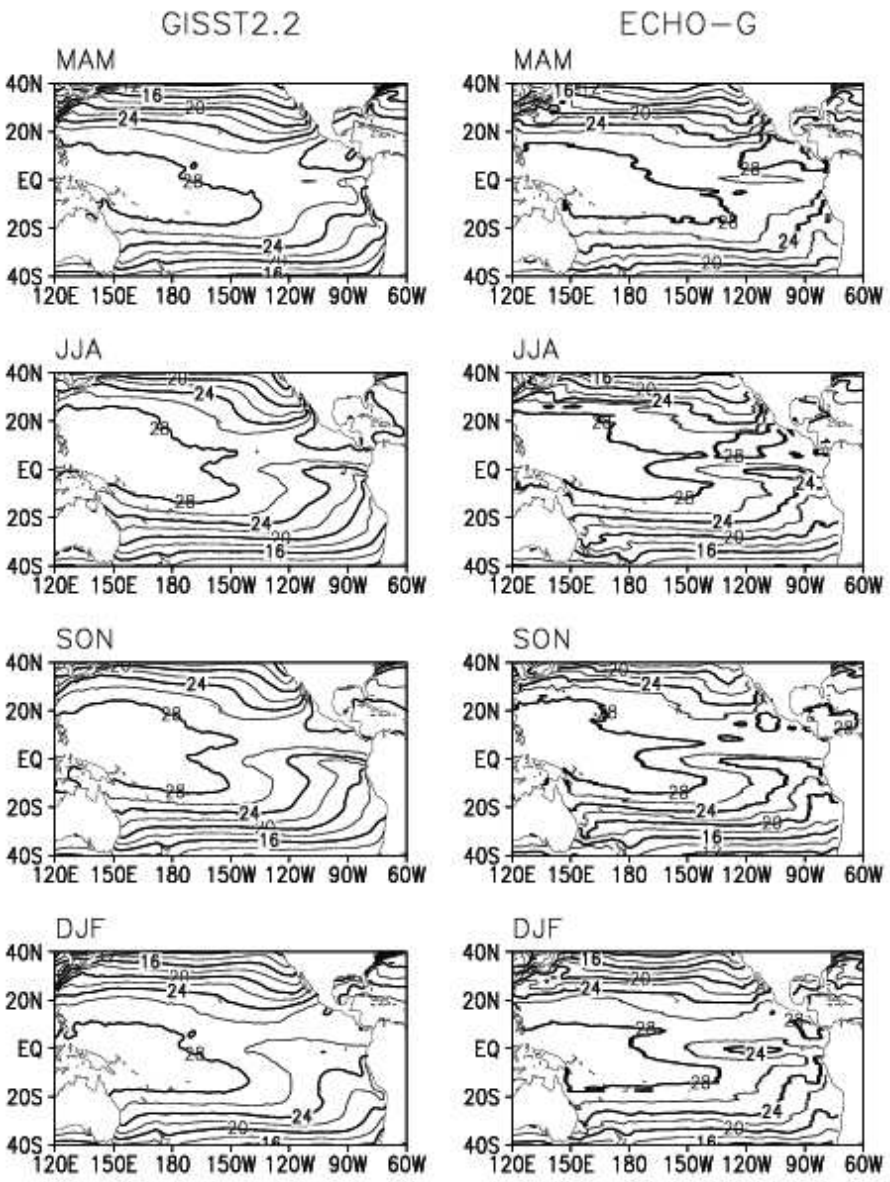

Figure 20 The Climatology of seasonal mean SST (°C) in the tropical Pacific for ECHO-G CTL (right) and GISST (1903-1994, left).

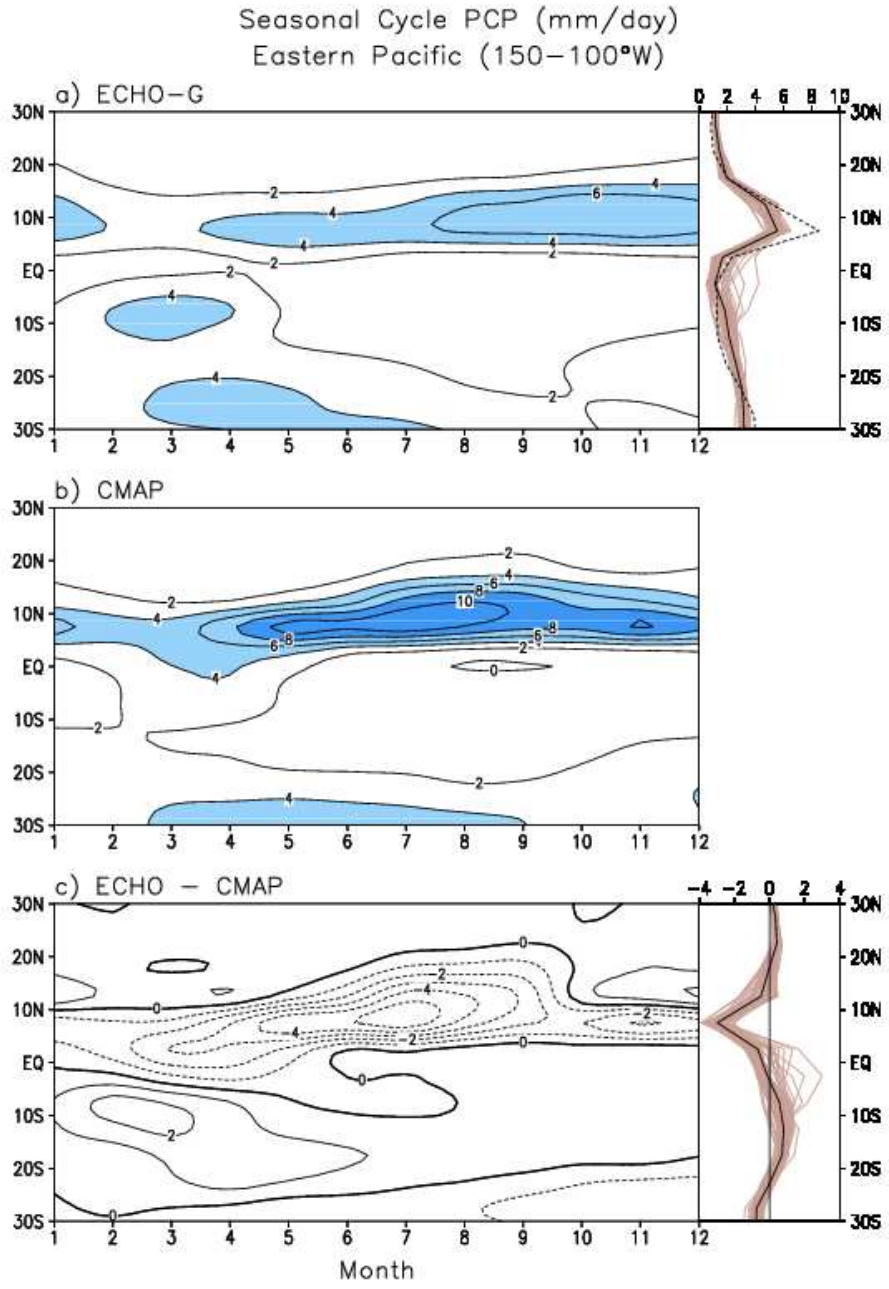

Figure 21 Annual cycle of precipitation (mm/day) in the tropical eastern Pacific (150-100°W) for a) ECHO-G CTL and b) CMAP (1979-1998) and c) their difference. Zonal means of the model (solid line) and the observation (dashed line) are plotted together in the right upper panel. The zonal mean of model biases is shown in the right lower panel. Light solid lines in zonal mean plots represent the results from 50 20-year subsections of ECHO-G CTL.

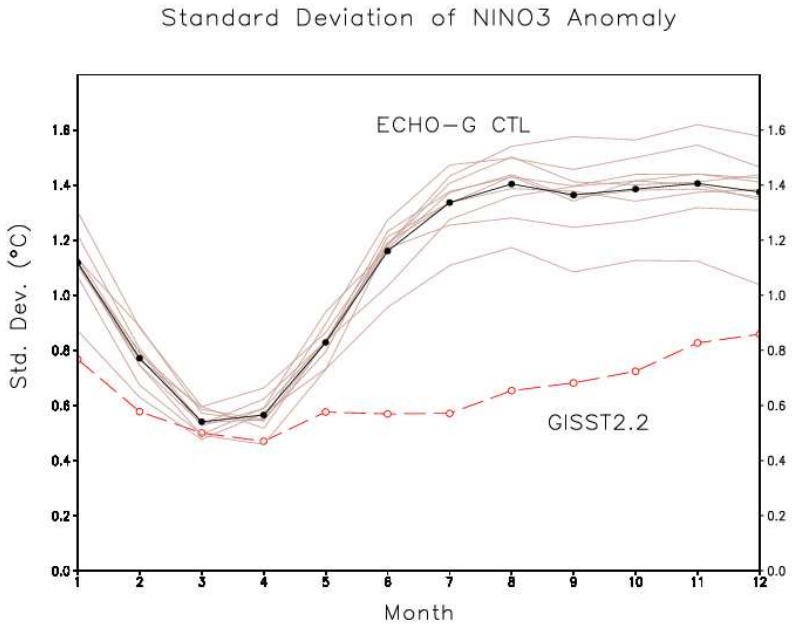

Figure 22 Monthly standard deviation of Niño3 SST (°C) for ECHO-G CTL and GISST (1903-1994). Light solid lines represent standard deviations from ten 92-year sections of ECHO-G CTL and the dark solid line is a mean of the ten standard deviations.

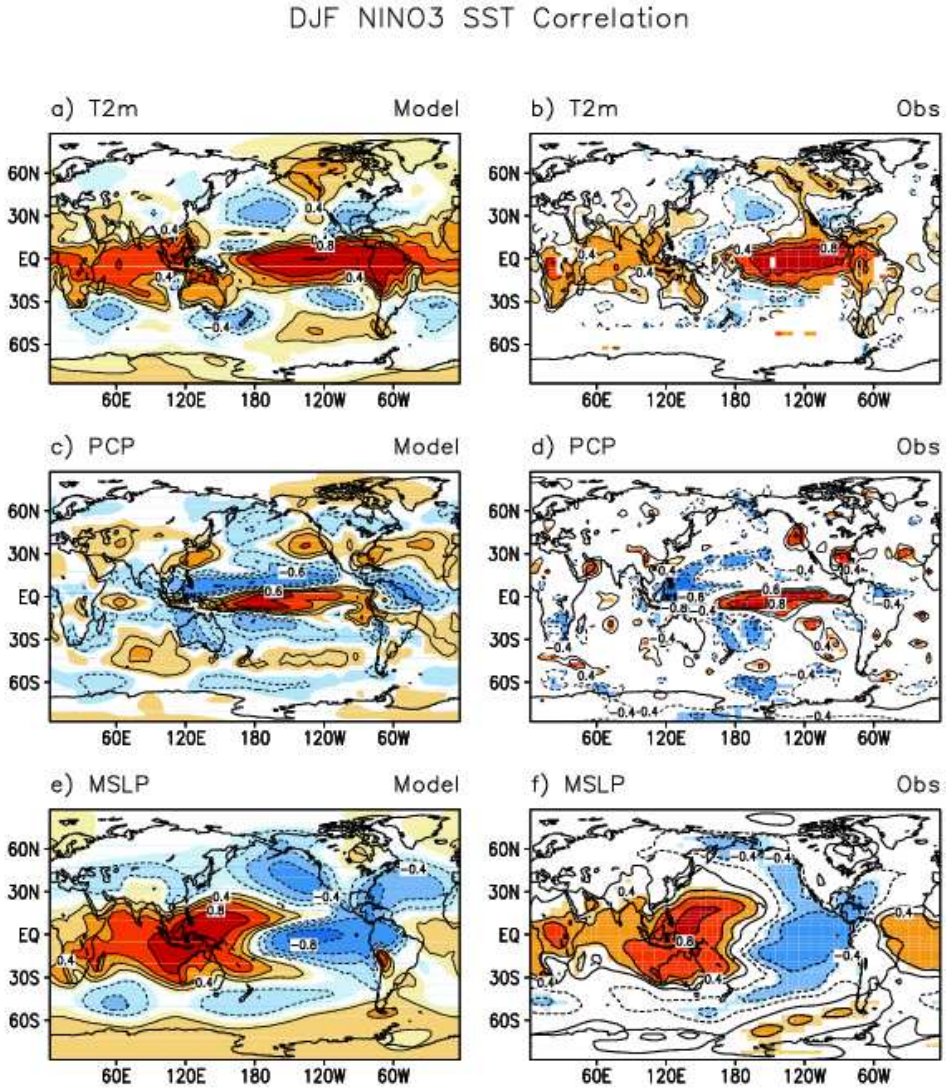

Figure 23 Correlation coefficients of DJF mean T2m (top), PCP (middle), and MSLP (bottom) with the DJF mean Niño3 index for ECHO-G (left) and observations (right). Contour intervals are 0.2 and zero lines are omitted. Contour lines of -0.2 and +0.2 are additionally left out in d). Shadings indicate areas where the correlation coefficients are statistically significant at 95% level (two-tailed t-test).

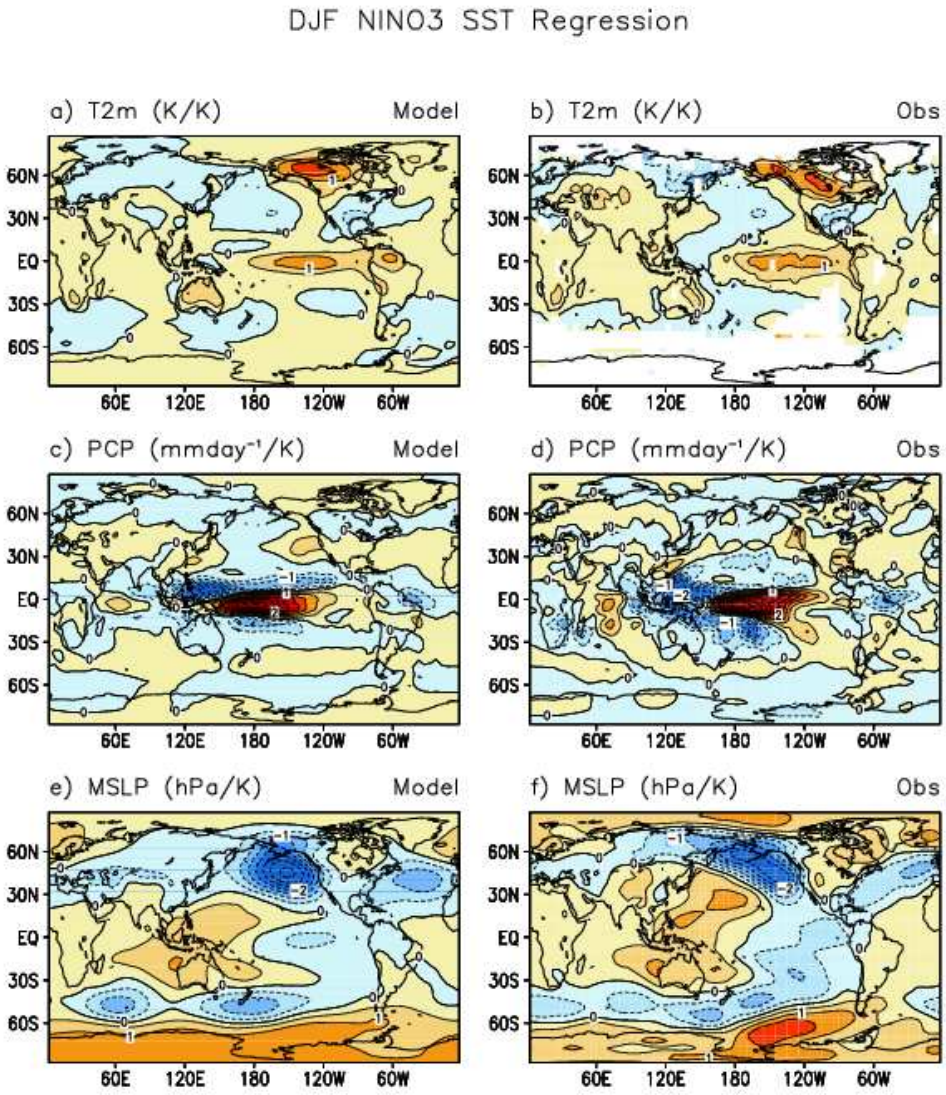

Figure 24 Same as Figure 23 but for regression coefficients. Contour intervals are 0.5.

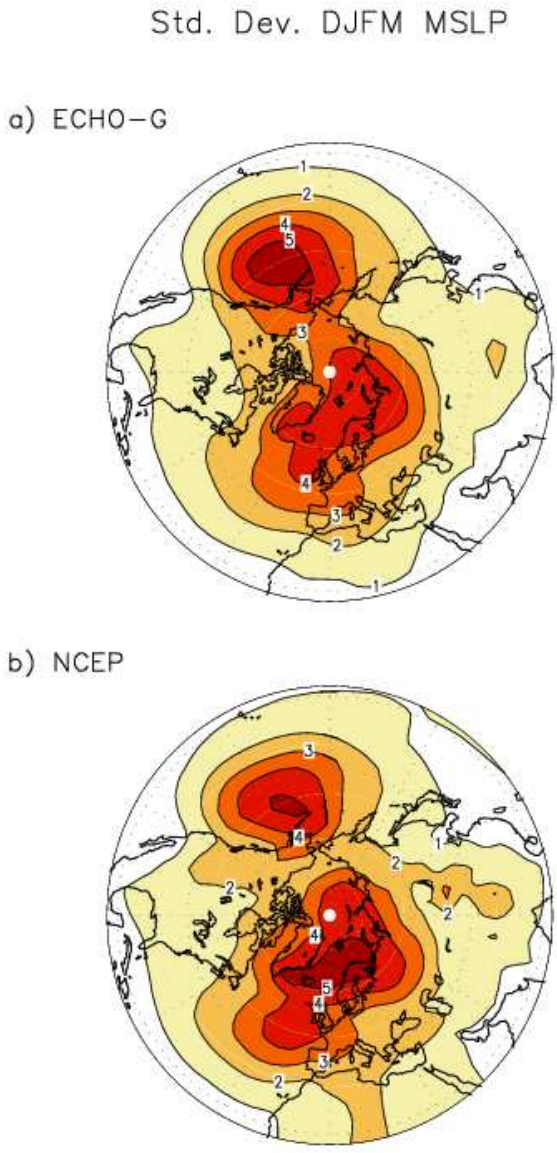

Figure 25 Spatial distribution of interannual standard deviation of DJFM MSLP (hPa) from a) ECHO-G CTL and b) NCEP/NCAR reanalysis (1958/59-2000/01).

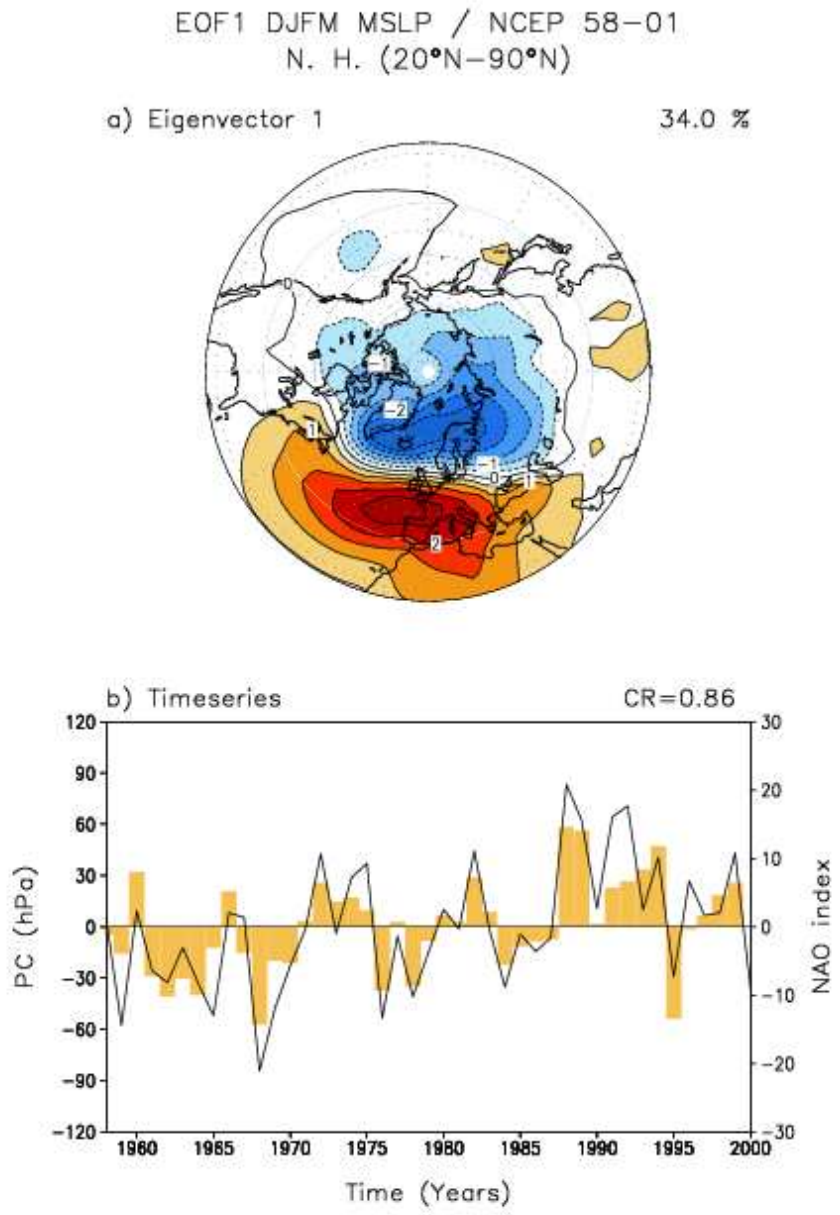

Figure 26 The leading PC of DJFM MSLP from NCEP/NCAR reanalysis (1958/59-2000/01): a) eigenvector and b) PC time series (solid line). Bars in b) represent the NAO index anomaly (hPa) which is defined as the Gibraltar minus Iceland DJFM mean MSLP difference (Jones et al. 1997). The eigenvector in a) has a unit of hPa by multiplying PC standard deviation to normalized eigenvector.

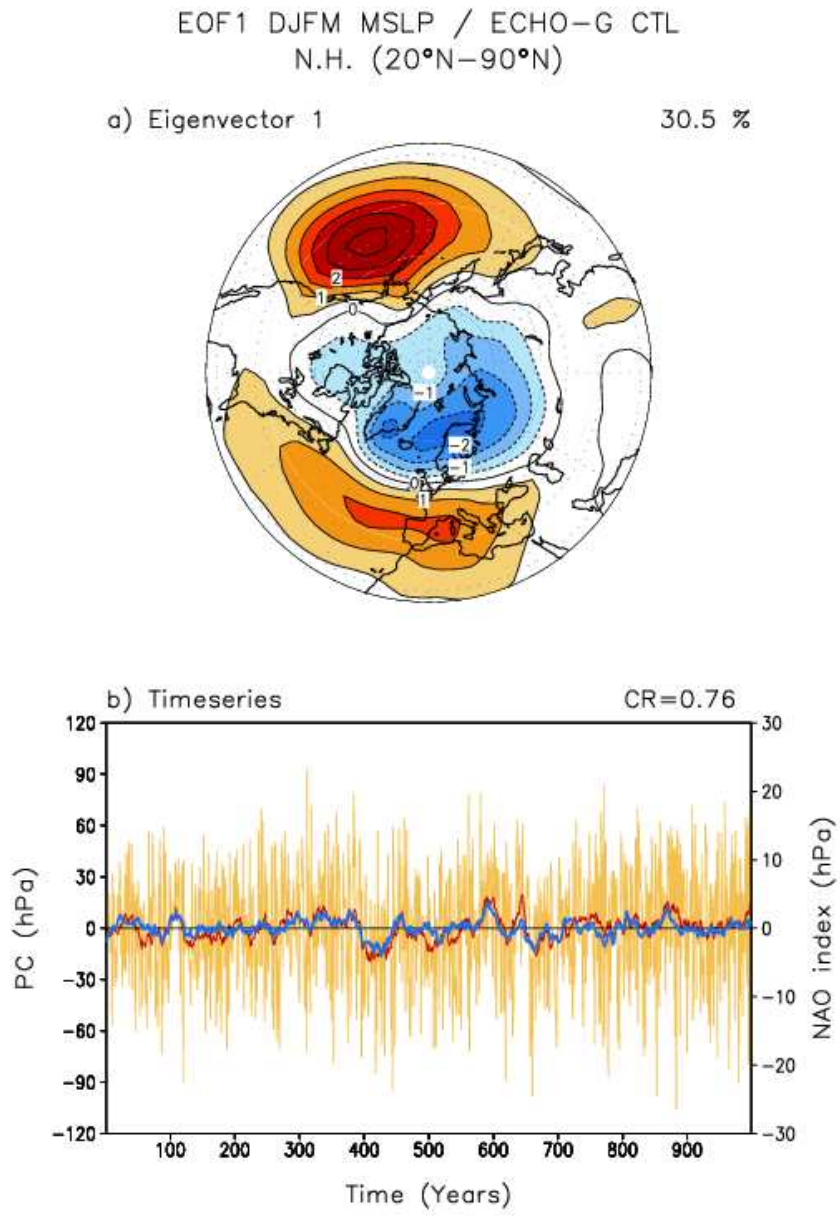

Figure 27 Same as Figure 26 but for ECHO-G CTL. In b) the light line is the principal component (PC), the thick blue dark line is a 11-year moving average of the PC, and the thin red dark line is a 11-year moving average of the NAO index anomaly (hPa).

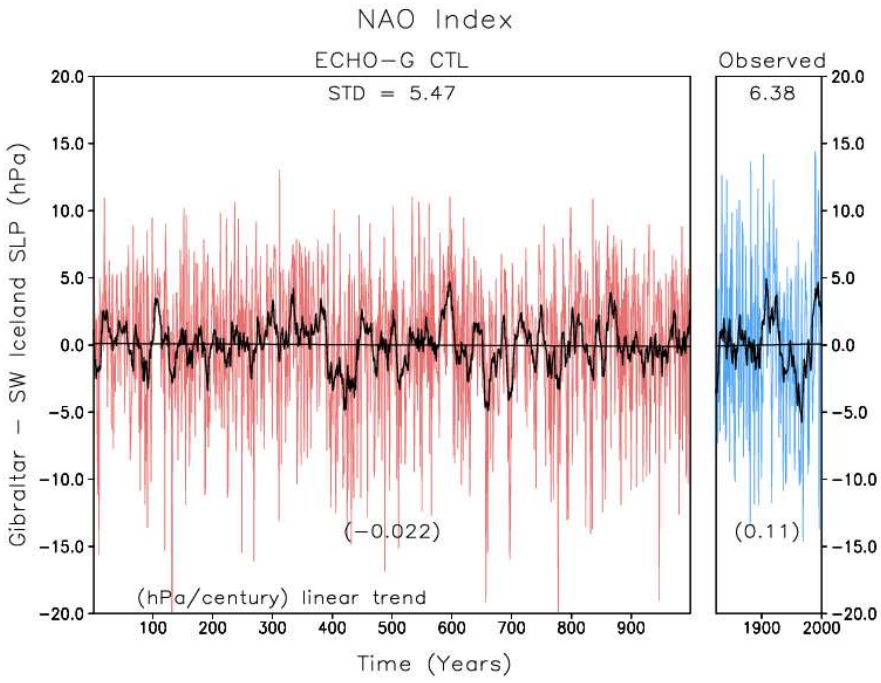

Figure 28 Time series of DJFM mean NAO index anomalies (thin lines) from ECHO-G CTL and observations (1825/26-2001/02). Solid lines are linear trends. Their values are given in parentheses (hPa/century). Thick lines are 11-year moving averages.

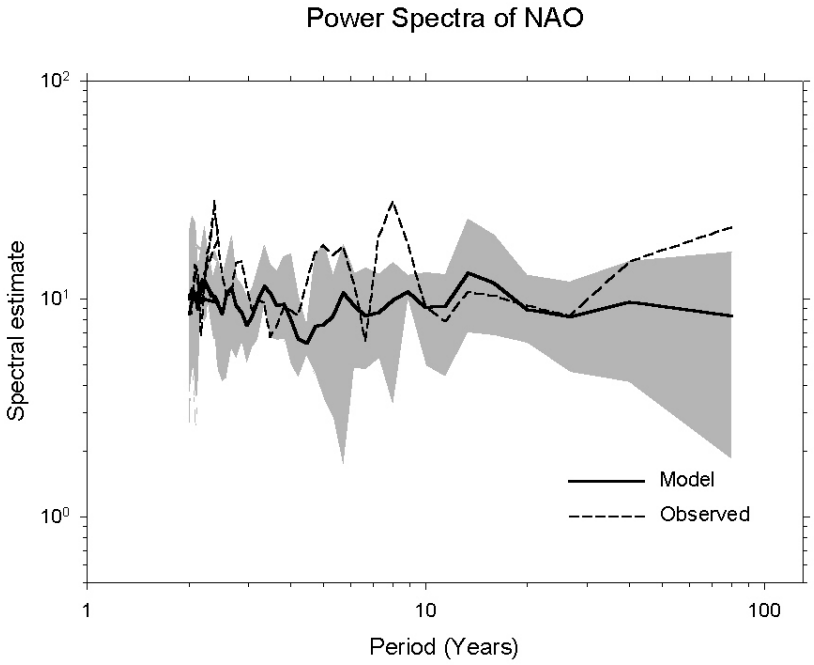

Figure 29 Same as Figure 3 but for DJFM NAO index. Five 177-year sections of ECHO-G CTL are used for the model spectra.

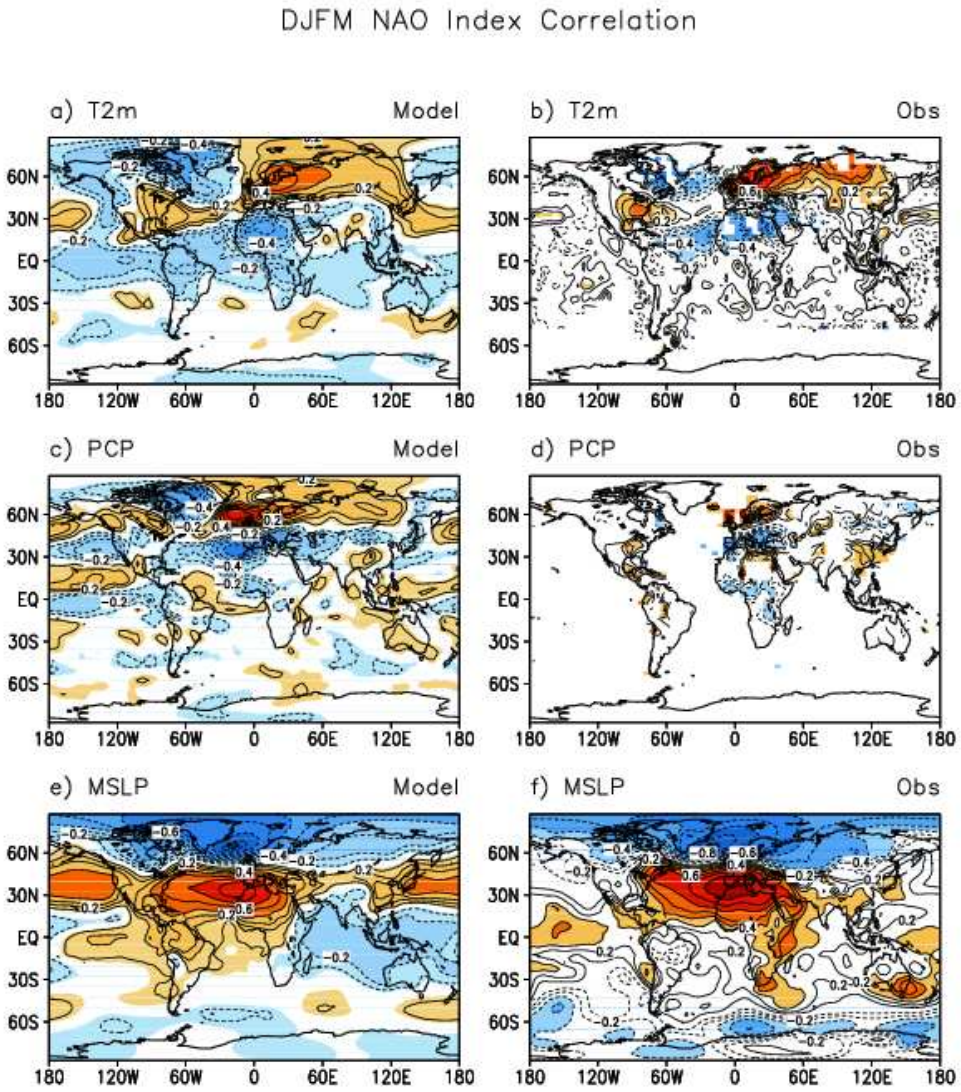

Figure 30 Spatial distribution of correlation coefficients with the DJFM mean NAO index for the observations (right panels) and model simulations (left panels): DJFM mean T2m (top), PCP (middle), and MSLP (bottom). Contour intervals are 0.1 and zero lines are omitted. Shadings represent the areas where the correlation coefficients are statistically significant at 95% level (two-tailed t-test).

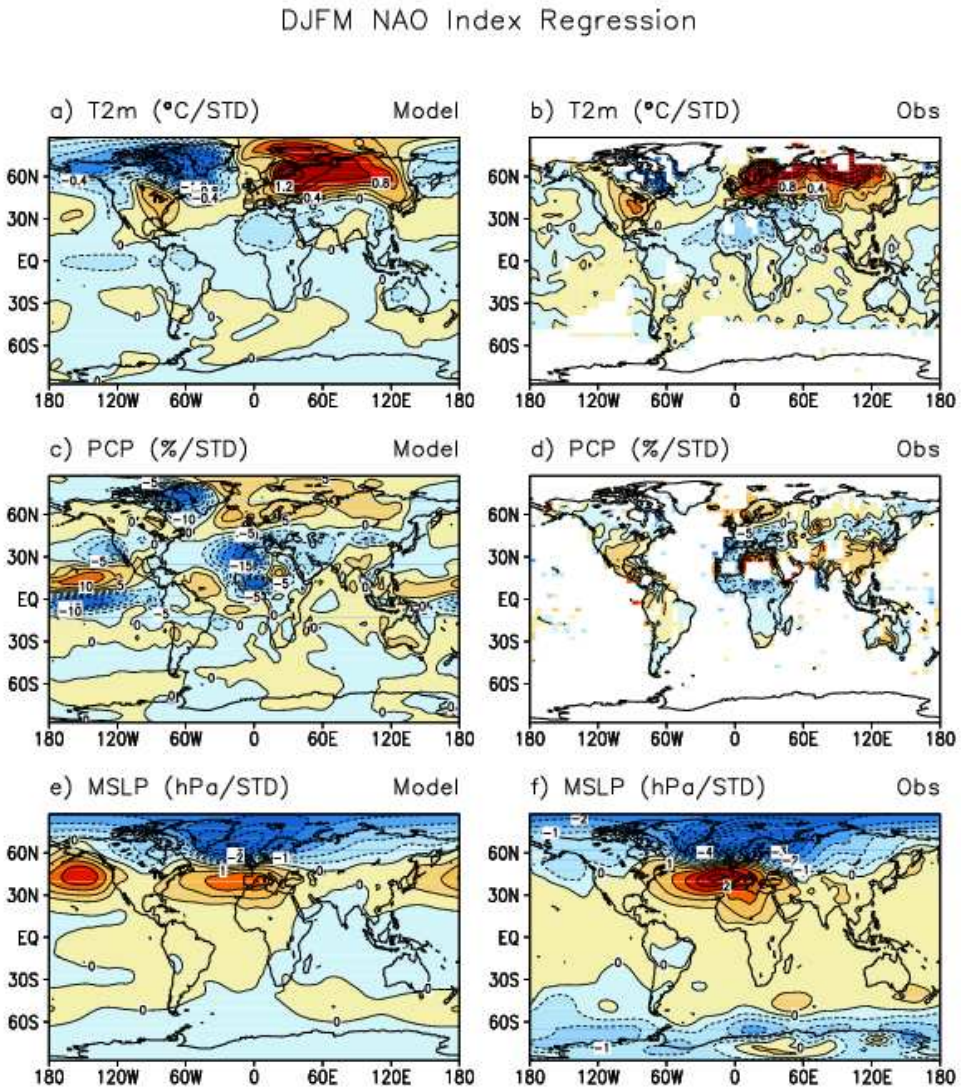

Figure 31 Same as Figure 30 but for the regression coefficients. Note that regression coefficients are normalized by the standard deviation (STD) of the NAO index. Contour intervals are 0.2°C/STD, 5 %/STD, and 0.5 hPa/STD for T2m, PCP, and MSLP, respectively.

Technical-Report-Reference: *Reprinted in

Report 1 - 2 Please order the reference list from **Modelle und Daten**
Max-Planck Institut für Meteorologie, Bundesstrasse 53, D-20146 Hamburg, Germany

Report No. 1 **The Adjoint of TM2**
December 2001 Michael Voßbeck, Thomas Kaminski, Ralf Giering, Martin Heimann

ISSN 1619-2257